

A unified theory for optimal feedforward torque control of anisotropic synchronous machines

Hisham Eldeeb^a, Christoph M. Hackl^{a,*}, Lorenz Horlbeck^b and Julian Kullick^a

^aResearch Group 'Control of Renewable Energy Systems (CRES)', Munich School of Engineering (MSE), Technical University of Munich (TUM), Munich, Germany; ^bInstitute of Automotive Technology (FTM), Technical University of Munich (TUM), Munich, Germany

ABSTRACT

A unified theory for optimal feedforward torque control of anisotropic synchronous machines with *non-negligible stator resistance* and *mutual inductance* is presented which allows to *analytically* compute (1) the optimal direct and quadrature reference currents for all operating strategies, such as maximum torque per current (MTPC), maximum current, field weakening, maximum torque per voltage (MTPV) or maximum torque per flux (MTPF), and (2) the transition points indicating when to switch between the operating strategies due to speed, voltage or current constraints. The analytical solutions allow for an (almost) instantaneous selection and computation of actual operation strategy and corresponding reference currents. Numerical methods (approximating these solutions only) are *no longer* required. The unified theory is based on one simple idea: all optimisation problems, their respective constraints and the computation of the intersection point(s) of voltage ellipse, current circle or torque, MTPC, MTPV, MTPF hyperbolas are reformulated implicitly as *quadratics* which allows to invoke the Lagrangian formalism and to find the roots of fourth-order polynomials analytically. The proposed theory is suitable for any anisotropic synchronous machine. Implementation and measurement results illustrate effectiveness and applicability of the theoretical findings in real world.

ARTICLE HISTORY

Received 18 March 2017
Accepted 31 May 2017

KEYWORDS

Maximum torque per ampere (MTPA); maximum torque per current (MTPC); maximum torque per voltage (MTPV); maximum torque per flux (MTPF); maximum current (MC); field weakening (FW); analytical solution; optimal feedforward torque control; efficiency; copper losses; anisotropy; synchronous machine; interior permanent-magnet synchronous machine; reluctance synchronous machine; permanent-magnet-assisted or enhanced synchronous machine; quadratics; quartics; Lagrangian optimisation; operation management

Notation

$\mathbb{N}, \mathbb{R}, \mathbb{C}$: natural, real, complex numbers. $\mathbf{x} := (x_1, \dots, x_n)^\top \in \mathbb{R}^n$: column vector, $n \in \mathbb{N}$ where ' \top ' and ' $:=$ ' mean 'transposed' (interchanging rows and columns of a matrix or vector) and 'is defined as', respectively. $\mathbf{0}_n \in \mathbb{R}^n$: zero vector. $\mathbf{a}^\top \mathbf{b} := a_1 b_1 + \dots + a_n b_n$: scalar product of the vectors $\mathbf{a} := (a_1, \dots, a_n)^\top$ and $\mathbf{b} := (b_1, \dots, b_n)^\top$. $\|\mathbf{x}\| := \sqrt{\mathbf{x}^\top \mathbf{x}} = \sqrt{x_1^2 + \dots + x_n^2}$: Euclidean norm of \mathbf{x} . $\mathbf{A} \in \mathbb{R}^{n \times n}$: (square) matrix with n rows and columns. \mathbf{A}^{-1} : inverse of \mathbf{A} (if exists). $\mathbf{A}^{-\top}$: inverse transpose of \mathbf{A} (if exists). $\det(\mathbf{A})$: determinant of \mathbf{A} , $\text{spec}(\mathbf{A})$: spectrum of \mathbf{A} (the set of the eigenvalues of \mathbf{A}). $\mathbf{I}_n \in \mathbb{R}^{n \times n} := \text{diag}(1, \dots, 1)$: identity matrix. $\mathbf{O}_{n \times p} \in \mathbb{R}^{n \times p}$: zero matrix, $n, p \in \mathbb{N}$.

$\mathbf{T}_p(\phi_k) = \begin{bmatrix} \cos(\phi_k) & -\sin(\phi_k) \\ \sin(\phi_k) & \cos(\phi_k) \end{bmatrix}$: park transformation matrix (with electrical angle ϕ_k) and $\mathbf{J} := \mathbf{T}_p(\pi/2) = \begin{bmatrix} 0 & -1 \\ 1 & 0 \end{bmatrix}$: rotation matrix (counter-clockwise rotation by $\frac{\pi}{2}$;

see e.g. Dirscherl, Hackl, & Schechner, 2015; Teodorescu, Liserre, & Rodríguez, 2011). 's.t.': subject to (optimisation with constraints). j : imaginary unit with $j^2 = \sqrt{-1}$, ' $\stackrel{!}{=}$ ': must equal. $X \cap Y$: intersection of the sets X and Y (in this paper: $X, Y \subset \mathbb{R}^2$).

1. Introduction

1.1 Motivation

Energy shortage and environmental impacts prompted engineers to improve the efficiency of electric drives; especially when studies indicated that electric machines consume more than half of the globally generated electricity (de Almeida, Ferreira, & Fong, 2011). Accordingly, major research and development advancements in the control and modelling of electric drives have been overseen. Special focus was set on permanent-magnet (PM)

CONTACT Christoph M. Hackl  christoph.hackl@tum.de

*Authors are in alphabetical order and contributed equally to the paper.

© 2017 The Author(s). Published by Informa UK Limited, trading as Taylor & Francis Group.

This is an Open Access article distributed under the terms of the Creative Commons Attribution-NonCommercial-NoDerivatives License (<http://creativecommons.org/licenses/by-nc-nd/4.0/>), which permits non-commercial re-use, distribution, and reproduction in any medium, provided the original work is properly cited, and is not altered, transformed, or built upon in any way.

synchronous motors (SMs) owing to their high power-density ratios, efficiency, flexibility and dynamic performance. It was explained in Morimoto, Takeda, Hirasa, and Taniguchi (1990), by considering the anisotropy of the PMSM rotor, one would be able to generate the same torque profile, as that obtained for *zero direct-axis* control, at a reduced magnitude of the stator current. As a matter of fact, this anisotropy laid the foundation for reluctance synchronous machines (RSMs). The anisotropy in the rotor introduces a high degree of saliency which could be manipulated through optimised rotor design to not only produce the necessary reluctance torque but also to generate a constant power speed range (compatible with field weakening (FW) operation; Wang, Ionel, Jiang, & Stretz, 2016). A hybrid machine that combines the merits of both PMSMs and RSMs (i.e. less rare-earth PM with high saliency ratio) is also known as PM-assisted RSM (PMA-RSM) (Boldea, Tutelea, Parsa, & Dorrell, 2014; Wang et al., 2016) or PM-enhanced RSM (PME-RSM) (Schmidt, 2014). Since copper losses dominate the electric losses for such machines, a reduction in the stator current magnitude, for a given load torque, will explicitly lead to higher efficiencies. Throughout this paper, the abbreviation ‘SMs’ will be used when referring to PMSMs, RSMs, PMA-RSMs or PME-RSMs. Two feasible approaches to enhance the efficiency of SMs are (1) improving the stator or rotor design (Boldea et al., 2014; Wang et al., 2016; Zhang, Ionel, & Demerdash, 2016) or (2) extracting the highest possible efficiency by optimising the adopted torque controller, which is the topic under study in this paper.

1.2 Literature review

The optimal feedforward torque control problem has been investigated in numerous publications: for maximum torque per ampere (MTPA) or maximum torque per current (MTPC¹), see e.g. Cavallaro et al. (2005), Cheng and Tesch (2010), Finken (2012), Gemassmer (2015), Jung, Hong, and Nam (2013), Lemmens, Vanassche, and Driesen (2015), Morimoto et al. (1990), Niazi, Toliyat, and Goodarzi (2007), Ni et al. (2015), Panaitescu and Topa (1998), Preindl and Bolognani (2015), Schröder (2009), Schoonhoven and Uddin (2016), Urasaki, Senjyu, and Uezato (2003); for FW, see e.g. Jung et al. (2013), Kim, Jeong, Nam, Yang, and Hwang (2015), Preindl and Bolognani (2013b), Preindl and Bolognani (2015), Schoonhoven and Uddin (2016), Zhang et al. (2016); and for maximum torque per voltage (MTPV), see e.g. Ahn et al. (2007), Horlbeck and Hackl (2016), Jung et al. (2013), Preindl and Bolognani (2013b), Tursini, Chiricozzi, and Petrella (2010), to name a few. Nevertheless, to

the best knowledge of the authors, a unified theory, which covers

- (a) all operation strategies (such as MTPC, maximum current (MC), FW, MTPV or maximum torque per flux (MTPF)) and
- (b) allows for an *analytical computation* of all respective optimal reference currents,
- (c) while stator resistance *and* mutual/cross-coupling inductance (magnetic cross-coupling) are explicitly considered,

is *not* yet available.

Initially, the operation of electric drives was optimised by seeking an operation close to a unity-power factor, where the ratio of input and output power (kW/kVA) implies efficient use of electrical energy (Nakamura, Kudo, Ishibashi, & Hibino, 1995). However, this does not necessarily imply that the electrical losses within the adopted machine are minimised (Mademlis, Kioskeridis, & Margaritis, 2004). Accordingly, this drove research to dig into the intrinsic nonlinear characteristics of SMs. Optimisation of torque production at *steady state* can be classified into two categories: (i) ‘search control’ (SC) and (ii) ‘loss model control’ (LMC). SC, in brief, is considered as a *perturb and observe* adaptive strategy, where a change in a control variable is carried out continuously, while observing the change in a predefined cost function (i.e. electrical losses). The optimal control input is selected if electrical losses are minimised. The SC method does not require precise knowledge of the machine parameters whilst converging to the optimal operating point that accounts for core and stator electrical losses (Vaez, John, & Rahman, 1997). Nevertheless, the stability of such a strategy is not always guaranteed and must be ensured through an additional stability network (Colby & Novotny, 1988). On the other hand, LMC – *adopted in this paper* – is based on the development of a mathematical model, which describes the electromagnetic conversion and the electrical losses of the SM throughout operation. Depending on such models, one or more control variables are defined. Such variables could be the load angle (i.e. angle between the direct axis and the Euclidean norm of the stator current vector) for PMA-RSMs (Niazi et al., 2007), stator flux linkage based on the converter duty cycle for RSMs (Foo & Zhang, 2016) and a *binary search algorithm* for IPMSMs (Cavallaro et al., 2005). Clearly, LMC strictly depends on the machine parameters which are sometimes provided by the manufacturer or can be obtained through experiments (Bedetti, Calligaro, & Petrella, 2016; Hackl, Kamper, Kullick, & Mitchell, 2016). Upon defining such a model for the employed SM, optimal control strategies are defined which can be classified into four

regions: *MTPC*, *MC* (operation on the current circle), *FW* and *MTPV* or *MTPF*. *MTPC* computes the optimal reference stator current vector that could generate the desired electromagnetic torque while copper losses are minimised up to a certain speed (Cavallaro et al., 2005; Cheng & Tesch, 2010; Finken, 2012; Gemassmer, 2015; Morimoto et al., 1990; Ni et al., 2015; Preindl & Bolognani, 2015; Schröder, 2009). *MC* allows to operate the SMs at its current limit (current circle). *FW* and *MTPV* (or *MTPF*) formulate the optimisation problem by searching for the optimal reference currents beyond rated speed and at saturated stator voltage (Kim et al., 2015; Preindl & Bolognani, 2013b, 2015; Zhang et al., 2016). All four operation strategies are pointed out later in more detail indicating the differences in terms of methodology and imposed assumptions.

For PMSMs (surface- or interior-mounted PMs), *MTPC* was proposed initially by formulating a convex optimisation problem, where an optimal current vector with minimum magnitude was computed without including the drive's voltage as a constraint (Panaitescu & Topa, 1998). The same control strategy could be mapped to PMA-RSM as the difference in models is not distinct (see Equations (1)–(4) in Section 2.1). Further enhancement for this *MTPC* depended on developing an iron loss model which, when coupled to the conventional *MTPC* in Panaitescu and Topa (1998), results in (slightly) better efficiency for high machine speeds. In Urasaki et al. (2003), the applied *MTPC* incorporates a simplified iron loss model based on root-mean-square calculations (for a constant iron loss resistance). The employed *MTPC* in Cavallaro et al. (2005) adopted an iron loss model represented with a variable resistance at different loading conditions. The highest efficiency enhancement recorded was 3.5% for the PMSM under test. In Ni et al. (2015), the authors discriminated between *MTPC* and their developed maximum torque per efficiency (MTPE), which is basically *MTPC* coupled with iron loss and inductance models extracted from finite element analysis (FEA) data that was available for the employed IPMSM. Even though, solely a 0.2 % efficiency gain was achieved, the availability of the necessary FEA data is not guaranteed for every IPMSM. Also, the polynomial fitting of the inductance models with the *direct* and *quadrature* (d, q)-stator current components was not discussed in detail. In Panaitescu and Topa (1998), Cavallaro et al. (2005), Preindl and Bolognani (2013a), Urasaki et al. (2003), Niazi et al. (2007) and Lemmens et al. (2015), the *MTPC* optimisation problems did not treat both the optimisation problem beyond rated speed and the effect of magnetic cross-coupling between the (d, q)-axes. Also, the optimal solutions were computed numerically, convergence and/or stability of

the algorithm is not entirely guaranteed. In Schoonhoven and Uddin (2016), the ability to obtain the optimal *MTPC* currents was demonstrated through Lyapunov stability analysis (assuming negligible magnetic cross-coupling). In Jung et al. (2013), an analytical expression for the optimal currents was obtained, while stator resistance and cross-coupling inductance were neglected in the voltage constraint and torque generation, respectively. For PMA-RSM, an additional fifth harmonic model was incorporated along with the fundamental (d, q)-model up to rated speed, which led to lower stator currents and improved performance (Niazi et al., 2007). An explicit expression for the optimal *MTPC* currents of RSMs was described in Ahn et al. (2007) neglecting the effect of magnetic cross-coupling in the electromagnetic torque.

The angular velocity is directly related to the applied stator voltage. In case the machine is required to rotate beyond nominal speed, the machine is said to be driven in *FW* mode. At such operating mode, the applied stator voltage saturates to its maximum value, while the (d, q)-current components are manipulated to account for the demanded torque (*if feasible*) coming from, for example, an outer speed control loop. The *FW* region is subdivided into two regimes, known as constant power and reduced power regimes. For PMSM and PMA-RSM, the admissible over-speed value as well as the power regimes (i.e. constant or reduced power regimes) are determined (Preindl & Bolognani, 2015; Zhang et al., 2016), depending on the drive capability of injecting the opposing characteristic current (i.e. the current to fully demagnetise the PM; Zhang et al., 2016) and the maximum speed from the mechanical point of view. As illustrated in Zhang et al. (2016), Lemmens et al. (2015) and Preindl and Bolognani (2013b, 2015), the applied voltage constraint at different speeds is represented in the (d, q)-plane by an ellipse, which determines whether or not the demanded torque is feasible. Depending on the actual speed and the corresponding feasible torque, the operating point of the machine is determined. Even though a robust *FW* optimal control strategy was presented in Schoonhoven and Uddin (2016), the effects of magnetic cross-coupling and stator resistance were neglected. In Tursini et al. (2010), the presented *FW* strategy takes into account the stator resistance with line approximation of the voltage limits at different speeds. The method calculates the approximated optimal currents with acceptable accuracy and reduced computational requirements as the operating point approaches the rated current limits. Otherwise, a significant error exists between the actual and approximated optimal currents (Horlbeck & Hackl, 2016). The discussed literature, so far, calculated the *FW* optimum currents numerically. In Jung et al. (2013), analytical *FW*

optimum currents were obtained for IPMSM, while the effects of the cross-coupling inductance were neglected. As for RSMs, the effect of considering both the stator resistance and core saturation on acquiring the corresponding optimal currents was depicted analytically in Ahn et al. (2007). However, the provided analytical solution was derived assuming that the machine operates on the MTPV current loci (i.e. current loci of the maximum admissible torque when the machine is driven beyond $\omega_{k,\text{cut-in}}^{\text{MTPV}}$ as explained in Section 4.4), which is not necessarily the practical case. Also, omitting the cross-coupling inductance shifts the locus of the voltage ellipse. It is worth to mention that the MTPF strategy minimises the stator iron losses at higher speeds based on the fact that iron losses become more significant at higher electrical angular velocities (Ni et al., 2015; Ueda, Morimoto, Inoue & Sanada, 2014). However, it is proven later in this paper that MTPF is a special case of MTPV. Also from a physical point of view, the anisotropic SM under study will always weaken the PM flux linkage (for PMSM, PMA-RSM or PME-RSM) or the stator flux linkage (for RSM), since all optimisation strategies inject a counteracting flux linkage by negative *direct-axis* currents, thus iron losses are implicitly reduced (Cavallaro et al., 2005). This assumption holds unless the machine is driven into much higher speeds (Kim et al., 2015).

1.3 Contributions of this paper

As discussed previously, to obtain the optimal currents corresponding to *non-zero* direct-axis control (i.e. MTPC and FW), numerical solutions are usually employed. Here, a trade-off between feasible convergence rate and guaranteed convergence should be considered for the choice of a suitable numerical method. Moreover, enhancing the outcome of such numerical solutions in general comes at the expense of tightening the programmed tolerances which may *decrease* the speed of the control algorithm and *increase* the computational load on the real-time system. It was explained explicitly in Ni et al. (2015, Section IV), Ahn et al. (2007, Section 2.2.3) and Ueda et al. (2014, Section II-B), that acquiring a general analytical solution of the optimal currents for MTPV and MTPF along with considering the stator resistance and magnetic cross-coupling is or seems *not possible* and would introduce a high degree of complexity.

Motivated by the aforementioned challenges and remaining open questions (e.g. how to consider stator resistance and cross-coupling inductance in the whole feedforward torque control problem), the following research work has been conducted. The main contributions of this paper are as follows:

- (i) The derivation of a *unified theory for optimal feedforward torque control for anisotropic (and isotropic) SMs* which allows to compute the optimal reference currents *analytically* for all operation strategies such as MTPC, MC, FW, MTPV or MTPF incorporating *stator resistance* and *cross-coupling (mutual) inductance* explicitly. To the best of the authors' knowledge, analytical solutions *including* stator resistance and mutual inductance for MTPC, MC, FW, MTPV or MTPF of anisotropic SMs are scarcely investigated or not available at all. Moreover, the proposed analytical solutions offer (a) guaranteed convergence to the optimal reference currents (compared to numerical methods), (b) easy and straightforward implementation, and (c) rapid execution and low computational burden making the proposed analytical algorithms very suitable even for modest (hence cheap) processor boards.
- (ii) The unified theory is established by (a) the use of *Lagrangian multipliers* and (b) an *implicit* problem formulation as *quadratics* (i.e. all trajectories of the constraints and operation strategies in the (d, q) -plane—such as current circle, voltage ellipse and torque hyperbola—are reformulated implicitly as quadric surfaces).
- (iii) It is shown that *only* for very high speeds or very small stator resistances, the MTPF solution is an acceptable approximation of the MTPV solution. In general, an MTPV algorithm incorporating stator resistance and mutual inductance yields higher efficiencies and should be preferably implemented (see also Eldeeb, Hackl, & Kullick, 2016).
- (iv) The negative effects of neglecting stator resistance and mutual inductance or both on the optimality of all operation strategies are illustrated, which show that neglecting these two parameters during optimisation will lead to significant deviations between optimal and approximated reference currents and, hence, to a reduction in achievable efficiency.
- (v) The analytical computation of the transition points indicating when to switch from one operation strategy to the other (e.g. from MTPC to FW or from MC to MTPV).
- (vi) The comparison of numerical and analytical solutions with respect to computation time. The analytical method is significantly faster.
- (vii) The real-time implementation of the proposed analytical solution for the MTPC problem for a highly nonlinear RSM. The measurement results illustrate effectiveness and applicability of the proposed method.

The remainder of the paper is organised as follows: **Section 2** revisits the dynamic model of anisotropic synchronous machines (SMs), the operation constraints (such as current and voltage constraint) and the problem formulation of optimal feedforward torque control. **Section 3** deals with mathematical preliminaries at steady state and the implicit reformulation of the optimisation problems and the machine constraints. This paves the way for **Section 4**, where the *analytical* solutions for MTPC, MC, FW, MTPV and MTPF are presented. **Section 5** defines the characteristic operating points at which the switching between the different optimal control strategies is carried out. **Section 6** demonstrates simulation and practical implementation results of the optimal control strategies explained in **Sections 4** and **5**. **Section 7** concludes the paper by a short summary and an outlook to future work. To improve readability, the mathematical derivations of the unified theory are collected and presented in **Appendices A.1–A.4**.

2. Problem statement

In this section, the dynamic model and the operation constraints of the considered SMs and the problem formulation are presented.

2.1 Generic dynamical model of synchronous machines (SMs)

The model of an anisotropic (a) permanent-magnet synchronous machine (PMSM) or (b) permanent-magnet-assisted or excited reluctance synchronous machine (PMA-RSM or PME-RSM, resp. Niazi et al., 2007; Schmidt, 2014) or (c) RSM in the (d, q) -reference frame² is given by

$$\left. \begin{aligned} \underbrace{\begin{pmatrix} u_s^d(t) \\ u_s^q(t) \end{pmatrix}}_{=: \mathbf{u}_s^k(t)} &= R_s \underbrace{\begin{pmatrix} i_s^d(t) \\ i_s^q(t) \end{pmatrix}}_{=: \mathbf{i}_s^k(t)} \\ &+ \omega_k(t) \begin{bmatrix} 0 & -1 \\ 1 & 0 \end{bmatrix} \underbrace{\begin{pmatrix} \psi_s^d(\mathbf{i}_s^k(t)) \\ \psi_s^q(\mathbf{i}_s^k(t)) \end{pmatrix}}_{=: \boldsymbol{\psi}_s^k(\mathbf{i}_s^k(t))} \\ &+ \frac{d}{dt} \boldsymbol{\psi}_s^k(\mathbf{i}_s^k(t)), \\ \frac{d}{dt} \omega_k(t) &= \frac{n_p}{\Theta} \left(m_m(\mathbf{i}_s^k(t)) - m_l(t) \right), \\ \frac{d}{dt} \phi_k(t) &= \omega_k(t), \end{aligned} \right\} \quad (1)$$

with initial values $\boldsymbol{\psi}_s^k(\mathbf{i}_s^k(0)) = \boldsymbol{\psi}_s^{k,0}$, $\omega_k(0) = \omega_m^0$ and $\phi_k(0) = \phi_m^0$. The following assumption is imposed on the flux linkage.

Assumption 2.1: For a (locally) constant inductance matrix $\mathbf{L}_s^k \in \mathbb{R}^{2 \times 2}$ (e.g. obtained by a linearisation of (1) at the actual operating point), the (local approximation of the) flux linkage can be expressed as follows (Hackl, 2015; Hackl, Kamper, Kullick, & Mitchell, 2015; Niazi et al., 2007; Schmidt, 2014):

$$\boldsymbol{\psi}_s^k(\mathbf{i}_s^k) = \underbrace{\begin{bmatrix} L_s^d & L_m \\ L_m & L_s^q \end{bmatrix}}_{=: \mathbf{L}_s^k \in \mathbb{R}^{2 \times 2}} \mathbf{i}_s^k + \underbrace{\begin{pmatrix} \psi_{pm}^d \\ \psi_{pm}^q \end{pmatrix}}_{=: \boldsymbol{\psi}_{pm}^k} \quad \text{where} \\ \boldsymbol{\psi}_{pm}^k = \begin{cases} (\psi_{pm}, 0)^\top, & \text{PMSM and PME-RSM,} \\ (0, -\psi_{pm})^\top, & \text{PMA-RSM, or} \\ (0, 0)^\top, & \text{RSM.} \end{cases} \quad (2)$$

Then, the machine torque can be computed as follows (argument t dropped for brevity):

$$\begin{aligned} m_m(\mathbf{i}_s^k) &= \frac{3}{2} n_p (\mathbf{i}_s^k)^\top \mathbf{J} \boldsymbol{\psi}_s^k(\mathbf{i}_s^k) \\ &\stackrel{(2)}{=} \frac{3}{2} n_p [(\mathbf{i}_s^k)^\top \mathbf{J} \mathbf{L}_s^k \mathbf{i}_s^k + (\mathbf{i}_s^k)^\top \mathbf{J} \boldsymbol{\psi}_{pm}^k] \end{aligned} \quad (3)$$

$$\begin{aligned} &= \frac{3}{2} n_p \left[\psi_{pm}^d i_s^q - \psi_{pm}^q i_s^d + (L_s^d - L_s^q) i_s^d i_s^q \right. \\ &\quad \left. + L_m ((i_s^q)^2 - (i_s^d)^2) \right] \end{aligned} \quad (4)$$

$$\stackrel{(2)}{=} \frac{3}{2} n_p \begin{cases} \left[\psi_{pm} i_s^q + (L_s^d - L_s^q) i_s^d i_s^q + L_m ((i_s^q)^2 - (i_s^d)^2) \right], \\ \quad \text{PMSM \& PME-RSM,} \\ \left[\psi_{pm} i_s^d + (L_s^d - L_s^q) i_s^d i_s^q + L_m ((i_s^q)^2 - (i_s^d)^2) \right], \\ \quad \text{PMA-RSM, or} \\ \left[(L_s^d - L_s^q) i_s^d i_s^q + L_m ((i_s^q)^2 - (i_s^d)^2) \right], \\ \quad \text{RSM.} \end{cases}$$

In (1)–(3) or (4), R_s (in Ω) is the stator resistance, $\mathbf{u}_s^k := (u_s^d, u_s^q)^\top$ (in V), $\mathbf{i}_s^k := (i_s^d, i_s^q)^\top$ (in A) and $\boldsymbol{\psi}_s^k := (\psi_s^d, \psi_s^q)^\top$ (in Wb) are stator voltage (e.g. applied by a voltage source inverter), current and flux linkage vectors in the (d, q) -reference frame, respectively. Note that $\omega_k = n_p \omega_m$ (in rad/s) and $\phi_k = n_p \phi_m$ are *electrical* angular frequency and angle, whereas ω_m and ϕ_m are *mechanical* angular frequency and angle of the rotor (with initial values ω_m^0 and ϕ_m^0), respectively. n_p is the pole pair number of the machine and Θ (in kg m^2) is the (rotor's) inertia. m_m is the electromagnetic machine torque³ and m_l (in Nm) is a (bounded) load torque.

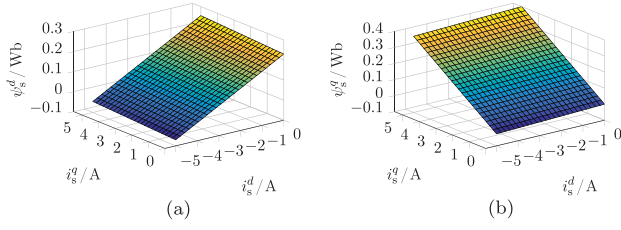


Figure 1. Flux linkage map (2) of an exemplary SM with parameters as in (36): (a) ψ_s^d -component and (b) ψ_s^q -component of the stator flux linkage. Due to the non-zero mutual inductance, both flux linkage maps are slightly tilted (the map is only shown for the second quadrant, i.e. $i_s^d \leq 0$ and $i_s^q \geq 0$).

The flux linkage ψ_s^k depends on the *symmetric, positive-definite* inductance matrix $\mathbf{L}_s^k = (\mathbf{L}_s^k)^\top > 0$ (Hackl, 2015) with stator inductances $L_s^q > 0$, $L_s^d > 0$ (both in H) and cross-coupling (mutual) inductance⁴ $L_m \in \mathbb{R}$ (in H) and $L_s^d L_s^q - L_m^2 > 0$, the stator currents i_s^k and the permanent-magnet flux linkage $\psi_{pm}^k = (\psi_{pm}^d, \psi_{pm}^q)^\top$. Figure 1 illustrates the flux linkage (2) of an anisotropic IPMSM for some exemplified values of L_s^q , L_s^d , L_m and ψ_{pm} .

Remark 2.1 (Affine flux linkage): Note that Assumption 2.1 implies a constant inductance matrix; this is in line with most recent publications (even from 2016) which also deal with constant inductances only (see e.g. Calleja, de Heredia, Gaztanaga, Nieva, & Aldasoro, 2016; Cavallaro et al., 2005; Lemmens et al., 2015; Preindl & Bolognani, 2013a; Preindl & Bolognani, 2013b, 2015; Tang, Li, Dusmez, & Akin, 2016, for PMSMs or Ahn et al., 2007; Foo & Zhang, 2016, for RSMs). This simplification will *not* be true in the most general case when the flux linkage is a nonlinear function of the currents (see e.g. Hackl et al., 2016). Nevertheless, in the humble opinion of the authors, the presented results are of quite some relevance and have not been discussed in this general framework before: the results of this paper can be considered as a generalisation of the results for IPMSM in Jung et al. (2013) by including resistance R_s and mutual inductance L_m into the generic optimisation formulation. The simplifying assumptions which neglect these physical parameters are overcome. Moreover, the presented results are applicable to *any* anisotropic SM (e.g. also to PMA-RSMs and RSMs) and, in Section 6, it is shown by measurement results that an application to a nonlinear RSM is feasible (for MTPC).

Remark 2.2 (Inductance ratios and signs of permanent-magnet flux linkage): For different machine designs, the direct and quadrature inductances take different values and have different ratios; also the permanent-magnet flux

constant changes its sign (Schmidt, 2014), i.e.

- PMSMs: $\psi_{pm}^d > 0$, $\psi_{pm}^q = 0$ and $L_s^q \geq L_s^d \Leftrightarrow \frac{L_s^d}{L_s^q} \leq 1$ (inverse saliency ratio);
- PME-RSMs: $\psi_{pm}^d > 0$, $\psi_{pm}^q = 0$ and (a) $L_s^q \geq L_s^d \Leftrightarrow \frac{L_s^d}{L_s^q} \leq 1$ (inverse saliency ratio) or (b) $L_s^q \leq L_s^d \Leftrightarrow \frac{L_s^d}{L_s^q} \geq 1$ (normal saliency ratio);
- PMA-RSMs with normal saliency: $\psi_{pm}^d = 0$, $\psi_{pm}^q < 0$ and $L_s^q \leq L_s^d \Leftrightarrow \frac{L_s^d}{L_s^q} \geq 1$ (normal saliency ratio); and
- RSMs: $\psi_{pm}^d = \psi_{pm}^q = 0$ and $L_s^q \leq L_s^d \Leftrightarrow \frac{L_s^d}{L_s^q} \geq 1$ (normal saliency ratio).

2.2 Operation constraints

Due to safety reasons (Schröder, 2009, Chapter 16), stator current and voltage vectors should never exceed their respective maximal *magnitudes* $\hat{i}_{max} > 0$ (in A) and $\hat{u}_{max} > 0$ (in V; both are amplitudes *not* RMS values here). Hence, the following must be ensured by the control system for all time:

$$\forall t \geq 0 \text{ s} : \quad \|\mathbf{i}_s^k(t)\|^2 \leq \hat{i}_{max}(t)^2 \quad \text{and} \quad \|\mathbf{u}_s^k(t)\|^2 \leq \hat{u}_{max}(t)^2. \quad (5)$$

Note that the maximally admissible current \hat{i}_{max} and voltage \hat{u}_{max} might change over time: (a) the current limit is usually equal to the nominal/rated current of the machine but can also exceed this nominal value for a short period in time and (b) the maximally applicable voltage will change with the DC-link voltage of the inverter. In the remainder of the paper, the time dependency will not be explicitly highlighted and the argument (t) will be dropped.

2.3 Problem formulation

For a given reference torque $m_{m,ref}$ (in N m) (and given current and voltage limits), the general objective is to find optimal and analytical solutions of the reference currents for all operation strategies such as MTPC, MC, FW, MTPV and MTPF. From a mathematical point of view, the following optimisation problem

$$\begin{aligned} & \max_{\mathbf{i}_s^k} -f(\mathbf{i}_s^k) \text{ s.t.} \\ & \left\{ \begin{array}{l} \|\mathbf{u}_s^k\| \leq \hat{u}_{max}, \|\mathbf{i}_s^k\| \leq \hat{i}_{max}, |m_m(\mathbf{i}_s^k)| \leq |m_{m,ref}| \\ \text{and } \text{sign}(m_{m,ref}) = \text{sign}(m_m(\mathbf{i}_s^k)), \end{array} \right. \end{aligned} \quad (6)$$

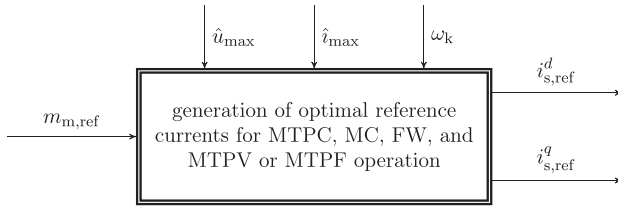


Figure 2. Optimal reference current generation for a given reference torque $m_{m,ref}$: the computed, optimal reference currents $i_{s,ref}^d$ and $i_{s,ref}^q$ depend also on maximal current \hat{i}_{max} , maximal voltage \hat{u}_{max} and (actual) electrical angular frequency $\omega_k = n_p \omega_m$.

with three inequality constraints and one equality constraint must be solved online, where obviously the sign of reference and machine torque should coincide. The function $f(\mathbf{i}_s^k)$ depends on the operation strategy (e.g. $f(\mathbf{i}_s^k) = \|\mathbf{i}_s^k\|^2$ for MTPC; for more details, see Section 4).

The most favourable outcome is an analytical solution which gives explicitly the reference current vector

$$\begin{aligned} & \mathbf{i}_{s,ref}^k(m_{m,ref}, \hat{u}_{max}, \hat{i}_{max}, \omega_k) \\ &= \begin{pmatrix} i_{s,ref}^d(m_{m,ref}, \hat{u}_{max}, \hat{i}_{max}, \omega_k) \\ i_{s,ref}^q(m_{m,ref}, \hat{u}_{max}, \hat{i}_{max}, \omega_k) \end{pmatrix} \\ &:= \arg \max_{\mathbf{i}_s^k} m_m(\mathbf{i}_s^k) \end{aligned} \quad (7)$$

as functions (see Figure 2) of reference torque $m_{m,ref}$ (coming from an outer control loop; e.g. the speed control loop), voltage limit \hat{u}_{max} , current limit \hat{i}_{max} and electrical angular velocity $\omega_k = n_p \omega_m$. The computed reference current vector $\mathbf{i}_{s,ref}^k$ can then directly be handed over to any underlying current controller.

Remark 2.3 (Feasible reference torques and non-convexity of the machine torque): Note that, due to the voltage limit (during high-speed operation) or, due to the current limit, the range of admissible reference torques is restricted. Hence, *not all* reference torques $m_{m,ref}$ are feasible during all operation modes; therefore, the additional inequality constraint in (6) must be considered. If the requested reference torque is feasible, the inequality constraint becomes the equality constraint $|m_m(\mathbf{i}_s^k)| = |m_{m,ref}|$ (or simply, $m_m(\mathbf{i}_s^k) = m_{m,ref}$). Important to note that the machine torque $m_m(\mathbf{i}_s^k) \propto (\mathbf{i}_s^k)^\top \mathbf{J} \mathbf{L}_s^k \mathbf{i}_s^k$ is *not* convex, since $\mathbf{J} \mathbf{L}_s^k = \begin{bmatrix} -L_m & -L_s^q \\ L_s^d & L_m \end{bmatrix}$ is non-symmetric and indefinite with eigenvalues $\pm \sqrt{L_m^2 - L_s^d L_s^q}$. Hence, maximising the machine torque is not a viable approach. To account for that, the general optimisation problem (6) will be divided into several sub-problems leading to the optimal operation strategies MTPC, MC, FW, MTPF or MTPV (see Sections 4 and 5).

3. Mathematical preliminaries

In this section, the steady-state model of the considered SMs is derived, and the machine torque and all operation constraints (such as current or voltage limit) are re-formulated *implicitly* as *quadratic surfaces (quadrics)*. This implicit forms will pave the way for the proposed theory of optimal feedforward torque control with analytical solution of the reference currents.

3.1 Steady-state operation

In the remainder of this paper, only steady-state operation is considered which implies that $\frac{d}{dt} \boldsymbol{\psi}_s^k(\mathbf{i}_s^k) = \frac{d}{dt} \mathbf{i}_s^k = \mathbf{0}_2$. This is justified since the reference torque is changing much slower than the current dynamics can produce the actual machine torque. Inserting (2) into (1) and neglecting the time derivative of the current, the steady-state stator circuit model of an SM in matrix/vector notation is obtained as follows:

$$\mathbf{u}_s^k = R_s \mathbf{i}_s^k + \omega_k \mathbf{J} \mathbf{L}_s^k \mathbf{i}_s^k + \omega_k \mathbf{J} \boldsymbol{\psi}_{pm}^k \quad (8)$$

where \mathbf{J} , and \mathbf{L}_s^k and $\boldsymbol{\psi}_{pm}^k$ are as in (1) and (2), respectively.

3.2 Implicit formulation of machine torque and constraints as quadrics

The steady-state SM model (8) will be the basis for all upcoming derivations. The trick to obtain and derive a unified theory for the optimal torque control problem under current and voltage constraints is the re-formulation of the general optimisation problem (6) *implicitly* by *quadrics (or quadric surfaces)* which will allow to invoke the Lagrangian formalism to derive analytical solutions for all operation strategies (such as MTPC, MTPV, FW, etc.). In the upcoming subsections, the implicit forms of torque hyperbola, voltage ellipse (elliptical area), current circle (circular area) and flux norm are presented. The explicit forms are also given (as link to the existing literature) if their expressions are not too long. Stator resistance $R_s \neq 0$ and mutual inductance $L_m \neq 0$ will *not* be neglected to present the most general result within the framework of affine flux linkages as in (2).

3.2.1 Torque hyperbola (constant torque trajectory)

To derive the implicit form as quadric of the torque hyperbola, the following symmetric matrix, vector and constant

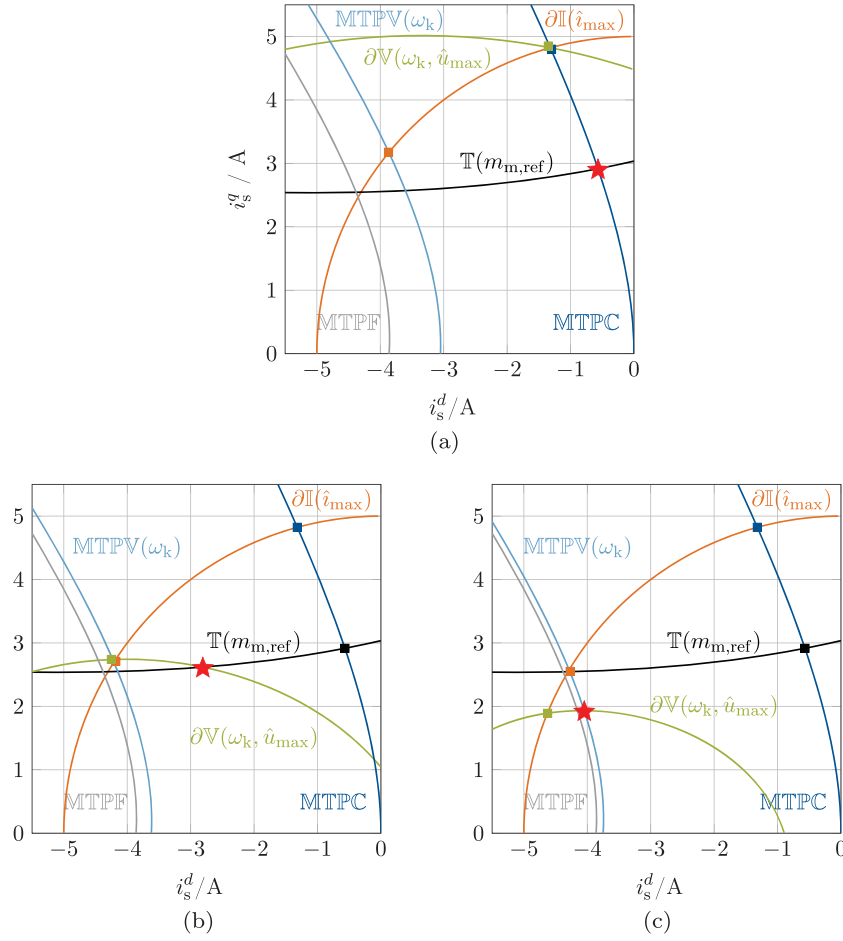


Figure 3. Illustration of three different feedforward torque control strategies for torque reference $m_{m,\text{ref}} > 0$ (second quadrant) and varying electrical angular velocities: (a) MTPC for $\omega_k = \omega_k^{\text{MC}} \leq \omega_{k,\text{nom}}$, i.e. $\text{MTPC} \cap \mathbb{T}(m_{m,\text{ref}})$, (b) FW for $\omega_{k,\text{nom}} < \omega_k = 2\omega_{k,\text{nom}} < \omega_{k,\text{cut-in}}^{\text{MTPV}}$, i.e. $\mathbb{T}(m_{m,\text{ref}}) \cap \partial\mathbb{V}(\omega_k, \hat{u}_{\text{max}})$ and (c) MTPV for $\omega_k = 3\omega_{k,\text{nom}} \geq \omega_{k,\text{cut-in}}^{\text{MTPV}}$ ($m_{m,\text{ref}}$ is not feasible anymore), i.e. $\text{MTPV}(\omega_k) \cap \partial\mathbb{V}(\omega_k, \hat{u}_{\text{max}})$: the three plots show voltage ellipse (—) $\partial\mathbb{V}(\omega_k, \hat{u}_{\text{max}})$, maximum current circle (—) $\partial\mathbb{I}(\hat{i}_{\text{max}})$, MTPC hyperbola (—) MTPC, torque hyperbola (—) $\mathbb{T}(m_{m,\text{ref}})$, MTPV hyperbola (—) $\text{MTPV}(\omega_k)$, MTPF hyperbola (—) MTPF and optimal operation point (★), respectively.

are defined:

$$\mathbf{T} := \frac{3}{4}n_p(\mathbf{J}\mathbf{L}_s^k + \mathbf{L}_s^k\mathbf{J}^\top) = \frac{3}{2}n_p \begin{bmatrix} -L_m & \frac{L_s^d - L_s^q}{2} \\ \frac{L_s^d - L_s^q}{2} & L_m \end{bmatrix} = \mathbf{T}^\top, \quad (9)$$

$$\mathbf{t} := \frac{3}{4}n_p\mathbf{J}\boldsymbol{\psi}_{\text{pm}}^k = \frac{3}{2}n_p \begin{pmatrix} -\frac{\psi_{\text{pm}}^q}{2} \\ \frac{\psi_{\text{pm}}^d}{2} \end{pmatrix}$$

$$\stackrel{(2)}{=} \begin{cases} \frac{3}{2}n_p \left(0, \frac{\psi_{\text{pm}}}{2}\right)^\top, & \text{PMSM and PME-RSM,} \\ \frac{3}{2}n_p \left(\frac{\psi_{\text{pm}}}{2}, 0\right)^\top, & \text{PMA-RSM, or} \\ (0, 0)^\top, & \text{RSM,} \end{cases}$$

$$\tau := \tau(m_{m,\text{ref}}) := -m_{m,\text{ref}}.$$

Moreover, note that $(\mathbf{i}_s^k)^\top \mathbf{J}\mathbf{L}_s^k \mathbf{i}_s^k = (\mathbf{i}_s^k)^\top \mathbf{L}_s^k \mathbf{J}^\top \mathbf{i}_s^k$, hence

$$\frac{3}{4}n_p(\mathbf{i}_s^k)^\top (\mathbf{J}\mathbf{L}_s^k + \mathbf{L}_s^k\mathbf{J}^\top) \mathbf{i}_s^k = (\mathbf{i}_s^k)^\top \mathbf{T} \mathbf{i}_s^k. \quad (10)$$

Now, by combining (9) and (10) with (3), the machine torque can be written as follows:

$$m_m(\mathbf{i}_s^k) = (\mathbf{i}_s^k)^\top \mathbf{T} \mathbf{i}_s^k + 2\mathbf{t}^\top \mathbf{i}_s^k. \quad (11)$$

For the machine torque $m_m(\mathbf{i}_s^k)$ as in (11) and a given constant reference torque $m_{m,\text{ref}}$, the machine torque hyperbola can be expressed implicitly as *quadratic* by invoking (9) as follows:

$$\mathbb{T}(m_{m,\text{ref}}) := \{ \mathbf{i}_s^k \in \mathbb{R}^2 \mid (\mathbf{i}_s^k)^\top \mathbf{T} \mathbf{i}_s^k + 2\mathbf{t}^\top \mathbf{i}_s^k + \tau(m_{m,\text{ref}}) = 0 \}. \quad (12)$$

An exemplary torque hyperbola is plotted in Figure 3 (see black line in Figure 3).

Remark 3.1 (Explicit expression for the torque hyperbola): For $i_s^d \leq 0$ and $m_{m,ref} > 0$, the torque hyperbola can be expressed explicitly (by solving (4) for i_s^q), i.e.

$$\mathbb{T}(i_s^d, m_{m,ref}) = \begin{cases} \frac{1}{3} \frac{3 \psi_{pm}^q n_p i_s^d + 2 m_{m,ref}}{n_p [\psi_{pm}^d + (L_s^d - L_s^q) i_s^d]}, & L_m = 0 \\ -\frac{(L_s^d - L_s^q) i_s^d + \psi_{pm}^d}{2 L_m} + \frac{\sqrt{M}}{2 L_m} & L_m \neq 0, \end{cases} \quad (13)$$

where $M := [(L_s^d - L_s^q)^2 + 4 L_m^2] (i_s^d)^2 + 2 \psi_{pm}^d (L_s^d - L_s^q) i_s^d + 4 L_m (i_s^d \psi_{pm}^q + \frac{2 m_{m,ref}}{3 p}) + (\psi_{pm}^d)^2$. Clearly, (13) holds for all $i_s^d \neq \psi_{pm} / (L_s^d - L_s^q)$. Note that the explicit expression in (13) relies on a case study for the mutual inductance (and the signs of current i_s^d and reference torque $m_{m,ref}$). The implicit form (12) holds in general and can easily be plotted (e.g. by using the command `ezplot` in Matlab).

3.2.2 Voltage elliptical area (reformulation of the voltage constraint in (5))

Recall that $\mathbf{J}^T \mathbf{J} = \mathbf{I}_2$, $\alpha^T = \alpha \in \mathbb{R}$ (the transpose of a scalar is the scalar itself), $(\mathbf{M}\mathbf{N})^T = \mathbf{N}^T \mathbf{M}^T$ (for matrices of appropriate size) and $(\mathbf{L}_s^k)^T = \mathbf{L}_s^k > 0$. With that in mind, inserting (8) into (5) and squaring the result yield

$$\begin{aligned} \hat{u}_{max}^2 &\stackrel{(5)}{\geq} \|\mathbf{u}_s^k\|^2 = (\mathbf{u}_s^k)^T \mathbf{u}_s^k = (u_s^d)^2 + (u_s^q)^2 \\ &\stackrel{(8)}{\geq} R_s^2 (\mathbf{i}_s^k)^T \mathbf{I}_2 \mathbf{i}_s^k + R_s \omega_k (\mathbf{i}_s^k)^T \mathbf{J} \mathbf{L}_s^k \mathbf{i}_s^k \\ &\quad + R_s \omega_k (\mathbf{i}_s^k)^T \mathbf{J} \psi_{pm}^k + \omega_k^2 (\mathbf{i}_s^k)^T \underbrace{(\mathbf{L}_s^k)^T \mathbf{J}^T \mathbf{J} \mathbf{L}_s^k}_{=(\mathbf{L}_s^k)^2} \mathbf{i}_s^k \\ &\quad + R_s \omega_k (\mathbf{i}_s^k)^T \mathbf{L}_s^k \mathbf{J}^T \mathbf{i}_s^k + \omega_k^2 (\mathbf{i}_s^k)^T (\mathbf{L}_s^k)^T \mathbf{J}^T \mathbf{J} \psi_{pm}^k \\ &\quad + R_s \omega_k (\psi_{pm}^k)^T \mathbf{J}^T \mathbf{i}_s^k + \omega_k^2 (\psi_{pm}^k)^T \mathbf{J}^T \mathbf{J} \mathbf{L}_s^k \mathbf{i}_s^k \\ &\quad + \omega_k^2 \underbrace{(\psi_{pm}^k)^T \mathbf{J}^T \mathbf{J} \psi_{pm}^k}_{=\|\psi_{pm}^k\|^2 = \psi_{pm}^2}. \end{aligned} \quad (14)$$

To find a more compact representation, the goal is to rewrite (14) as a quadric. Therefore, in (14), terms of the form $(\mathbf{i}_s^k)^T \square \mathbf{i}_s^k$ and $\square^T \mathbf{i}_s^k$ (where \square is either a matrix or a vector) are collected. Then, by defining the following

matrix, vector and scalar

$$\begin{aligned} \mathbf{V}(\omega_k) &:= \begin{bmatrix} v_{11}(\omega_k), v_{12}(\omega_k) \\ v_{12}(\omega_k), v_{22}(\omega_k) \end{bmatrix} \\ &= R_s^2 \mathbf{I}_2 + R_s \omega_k (\mathbf{J} \mathbf{L}_s^k + \mathbf{L}_s^k \mathbf{J}^T) \\ &\quad + \omega_k^2 (\mathbf{L}_s^k)^2 = \mathbf{V}(\omega_k)^T \\ &= \begin{bmatrix} R_s^2 - 2 \omega_k R_s L_m + \omega_k^2 [(L_s^d)^2 + L_m^2], \\ \omega_k R_s (L_s^d - L_s^q) + \omega_k^2 L_m (L_s^d + L_s^q), \\ \omega_k R_s (L_s^d - L_s^q) + \omega_k^2 L_m (L_s^d + L_s^q), \\ R_s^2 + 2 \omega_k R_s L_m + \omega_k^2 [(L_s^q)^2 + L_m^2] \end{bmatrix}, \\ \mathbf{v}(\omega_k)^T &:= \begin{pmatrix} v_1(\omega_k) \\ v_2(\omega_k) \end{pmatrix} = \omega_k (\psi_{pm}^k)^T (\omega_k \mathbf{L}_s^k + R_s \mathbf{J}^T) \\ &\stackrel{(2)}{=} \begin{cases} \begin{pmatrix} \omega_k^2 L_s^d \psi_{pm} \\ \omega_k \psi_{pm} (R_s + \omega_k L_m) \end{pmatrix}^T, & \text{PMSM and PME-RSM,} \\ \begin{pmatrix} -\omega_k \psi_{pm} (R_s - \omega_k L_m) \\ \omega_k^2 L_s^q \psi_{pm} \end{pmatrix}^T, & \text{PMA-RSM, or} \\ (0, 0), & \text{RSM} \end{cases} \\ \nu(\omega_k) &:= \nu(\omega_k, \hat{u}_{max}) := \omega_k^2 (\psi_{pm}^k)^T \mathbf{J}^T \mathbf{J} \psi_{pm}^k - \hat{u}_{max}^2 \\ &\stackrel{(2)}{=} \begin{cases} \omega_k^2 \psi_{pm}^2 - \hat{u}_{max}^2, & \text{PMSM, PME-RSM or PMA-RSM,} \\ -\hat{u}_{max}^2, & \text{RSM,} \end{cases} \end{aligned} \quad (15)$$

the voltage constraint in (14) (or in (5)) can be expressed as follows:

$$\|\mathbf{u}_s^k\|^2 - \hat{u}_{max}^2 \stackrel{(14),(15)}{=} (\mathbf{i}_s^k)^T \mathbf{V}(\omega_k) \mathbf{i}_s^k + 2 \mathbf{v}(\omega_k)^T \mathbf{i}_s^k + \nu(\omega_k, \hat{u}_{max}) \leq 0.$$

Finally, the voltage constraint (14) can be written implicitly as quadric surface defined by

$$\mathbb{V}(\omega_k, \hat{u}_{max}) := \{ \mathbf{i}_s^k \in \mathbb{R}^2 \mid (\mathbf{i}_s^k)^T \mathbf{V}(\omega_k) \mathbf{i}_s^k + 2 \mathbf{v}(\omega_k)^T \mathbf{i}_s^k + \nu(\omega_k, \hat{u}_{max}) \leq 0 \}, \quad (16)$$

which describes the *voltage elliptical area*. The *voltage ellipse* is given by

$$\begin{aligned} \partial \mathbb{V}(\omega_k, \hat{u}_{max}) &:= \{ \mathbf{i}_s^k \in \mathbb{R}^2 \mid \underbrace{(\mathbf{i}_s^k)^T \mathbf{V}(\omega_k) \mathbf{i}_s^k + 2 \mathbf{v}(\omega_k)^T \mathbf{i}_s^k + \nu(\omega_k, \hat{u}_{max})}_{=: Q_{\partial \mathbb{V}}(\mathbf{i}_s^k, \omega_k, \hat{u}_{max})} = 0 \}, \end{aligned} \quad (17)$$

and describes the boundary of the elliptical area (16) (see green line (—) in Figure 3). Since $\mathbf{V}(\omega_k)$, $\mathbf{v}(\omega_k)$ and $\nu(\omega_k, \hat{u}_{max})$ explicitly depend on the electrical angular

velocity ω_k , the quadric $Q_{\partial\mathbb{V}}(\mathbf{i}_s^k, \omega_k, \hat{u}_{\max})$ of the voltage ellipse clearly depends on currents $\mathbf{i}_s^k = (i_s^d, i_s^q)^\top$, angular velocity ω_k and voltage limit \hat{u}_{\max} , and hence will move in the current locus for varying angular velocities.

Remark 3.2 (Symmetry of expression for the torque hyperbola): $V(\omega_k)$: Note that the matrix $V(\omega_k) = V(\omega_k)^\top \in \mathbb{R}^{2 \times 2}$ is *indeed* symmetric for all $\omega_k \in \mathbb{R}$, since all its sub-matrices are symmetric, respectively, i.e. $(R_s \mathbf{I}_2)^\top = R_s \mathbf{I}_2$, $(\mathbf{J} \mathbf{L}_s^k + \mathbf{L}_s^k \mathbf{J}^\top)^\top = (\mathbf{J} \mathbf{L}_s^k)^\top + (\mathbf{L}_s^k \mathbf{J}^\top)^\top = \mathbf{L}_s^k \mathbf{J}^\top + \mathbf{J} \mathbf{L}_s^k = \begin{bmatrix} -2L_m & L_s^d - L_s^q \\ L_s^d - L_s^q & 2L_m \end{bmatrix}$ and $((\mathbf{L}_s^k)^2)^\top = ((\mathbf{L}_s^k)^\top \mathbf{L}_s^k)^\top = (\mathbf{L}_s^k)^\top \mathbf{L}_s^k = (\mathbf{L}_s^k)^2 = \begin{bmatrix} (L_s^d)^2 + L_m^2 & L_m(L_s^d + L_s^q) \\ L_m(L_s^d + L_s^q) & (L_s^q)^2 + L_m^2 \end{bmatrix}$.

3.2.3 Current circular area (reformulation of the current constraint in (5))

The current constraint in (5) can also be expressed implicitly as quadric as follows:

$$\mathbb{I}(\hat{i}_{\max}) := \{ \mathbf{i}_s^k \in \mathbb{R}^2 \mid (\mathbf{i}_s^k)^\top \mathbf{I}_2 \mathbf{i}_s^k - \hat{i}_{\max}^2 \leq 0 \} \quad (18)$$

which describes the admissible *MC circular area*: the magnitude of the stator current vector must not exceed the current limit \hat{i}_{\max} . The *MC circle* (see orange line (—)) in Figure 3, i.e. the boundary of (18), is given by

$$\partial\mathbb{I}(\hat{i}_{\max}) := \{ \mathbf{i}_s^k \in \mathbb{R}^2 \mid (\mathbf{i}_s^k)^\top \mathbf{I}_2 \mathbf{i}_s^k - \hat{i}_{\max}^2 = 0 \}. \quad (19)$$

Remark 3.3 (Explicit expression for the MC circle): The current circle is given by $i_s^q = \pm \sqrt{\hat{i}_{\max}^2 - (i_s^d)^2}$.

3.2.4 Norm of the flux linkage

To operate the machine in MTPF mode, the squared norm of the flux linkage is minimised. The flux norm can also be expressed as quadric as follows:

$$\begin{aligned} \|\boldsymbol{\psi}_{\text{pm}}^k\|^2 &\stackrel{(2)}{=} (\mathbf{L}_s^k \mathbf{i}_s^k + \boldsymbol{\psi}_{\text{pm}}^k)^\top (\mathbf{L}_s^k \mathbf{i}_s^k + \boldsymbol{\psi}_{\text{pm}}^k) \\ &=: (\mathbf{i}_s^k)^\top \mathbf{F} \mathbf{i}_s^k + 2\mathbf{f} \mathbf{i}_s^k + \phi, \end{aligned} \quad (20)$$

where

$$\begin{aligned} \mathbf{F} &:= (\mathbf{L}_s^k)^2 = \begin{bmatrix} (L_s^d)^2 + L_m^2 & L_m(L_s^d + L_s^q) \\ L_m(L_s^d + L_s^q) & (L_s^q)^2 + L_m^2 \end{bmatrix} = \mathbf{F}^\top, \\ \mathbf{f} &:= \mathbf{L}_s^k \boldsymbol{\psi}_{\text{pm}}^k \stackrel{(2)}{=} \begin{cases} \boldsymbol{\psi}_{\text{pm}}(L_s^d, L_m)^\top, & \text{PMSM and} \\ & \text{PME-RSM,} \\ \boldsymbol{\psi}_{\text{pm}}(L_m, L_s^q)^\top, & \text{PMA-RSM, or} \\ (0, 0)^\top, & \text{RSM,} \end{cases} \\ \phi &:= (\boldsymbol{\psi}_{\text{pm}}^k)^\top \boldsymbol{\psi}_{\text{pm}}^k = \|\boldsymbol{\psi}_{\text{pm}}^k\|^2 \\ &\stackrel{(2)}{=} \begin{cases} \psi_{\text{pm}}^2, & \text{PMSM, PME-RSM and PMA-RSM,} \\ 0, & \text{RSM,} \end{cases} \end{aligned} \quad (21)$$

are the corresponding matrix, vector and scalar of the flux linkage quadric.

4. Operation strategies

In this section, the operation strategies MTPC, MC, FW, MTPV and MTPF are discussed in more detail, and the analytical solutions for the respective reference currents are presented. Finally, the operation strategies are explained based on the visualisation of the current loci (see Figure 3). The significant impact of neglecting stator resistance and mutual inductance on the efficiency of the machine is discussed and illustrated (see Figure 4).

4.1 Maximum torque per current (MTPC) hyperbola (considering L_m)

For low speeds, the voltage constraint in (5) is *not* critical. The current constraint in (5) and the minimisation of (copper) losses dominate the operation of the machine which requires the use of the MTPC strategy (or mostly called MTPA (Schröder, 2009, Section 16.7.1) or (Cavallaro et al., 2005; Kim et al., 2015, Preindl & Bolognani, 2015)). The MTPC optimisation problem is formulated as follows:

$$\begin{aligned} \max_{\mathbf{i}_s^k \in \mathbb{S}} -\|\mathbf{i}_s^k\|^2 \quad \text{s.t.} \quad m_m(\mathbf{i}_s^k) &= (\mathbf{i}_s^k)^\top \mathbf{T} \mathbf{i}_s^k + 2\mathbf{t}^\top (\mathbf{i}_s^k) \\ &\stackrel{!}{=} m_{m,\text{ref}} \stackrel{(9)}{=} -\tau(m_{m,\text{ref}}) \end{aligned} \quad (22)$$

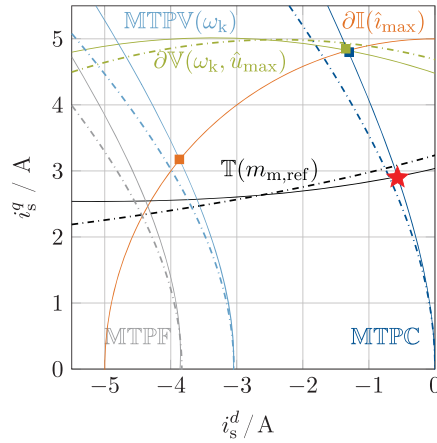
with $\mathbb{S} := \mathbb{V}(\omega_k, \hat{u}_{\max}) \cap \mathbb{I}(\hat{i}_{\max})$. The admissible solution set \mathbb{S} is the intersection of voltage elliptical area $\mathbb{V}(\omega_k, \hat{u}_{\max})$ and current circular area $\mathbb{I}(\hat{i}_{\max})$. Its solution, the MTPC hyperbola (see blue line (—)) in Figure 3, is given by the quadric

$$\text{MTPC} := \{ \mathbf{i}_s^k \in \mathbb{R}^2 \mid (\mathbf{i}_s^k)^\top \mathbf{M}_C \mathbf{i}_s^k + 2\mathbf{m}_C^\top \mathbf{i}_s^k = 0 \} \quad (23)$$

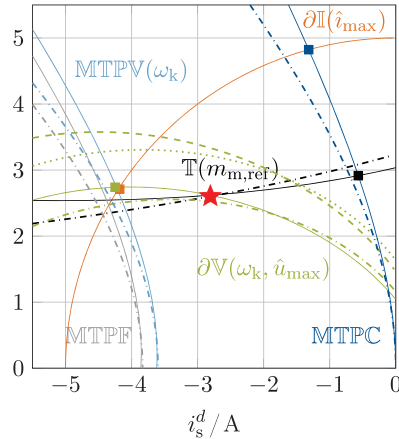
where

$$\begin{aligned} \mathbf{M}_C &:= \frac{3}{2} n_p \begin{bmatrix} \frac{L_s^d - L_s^q}{2} & L_m \\ L_m & -\frac{L_s^d - L_s^q}{2} \end{bmatrix} = \mathbf{M}_C^\top \quad \text{and} \\ \mathbf{m}_C &:= \frac{3}{2} n_p \begin{pmatrix} \frac{\psi_{\text{pm}}^d}{4} \\ \frac{\psi_{\text{pm}}^q}{4} \end{pmatrix} \\ &\stackrel{(2)}{=} \begin{cases} \frac{3}{2} n_p (\boldsymbol{\psi}_{\text{pm}}, 0)^\top, & \text{PMSM and PME-RSM} \\ \frac{3}{2} n_p (0, \boldsymbol{\psi}_{\text{pm}})^\top, & \text{PMA-RSM, or} \\ (0, 0)^\top, & \text{RSM.} \end{cases} \end{aligned} \quad (24)$$

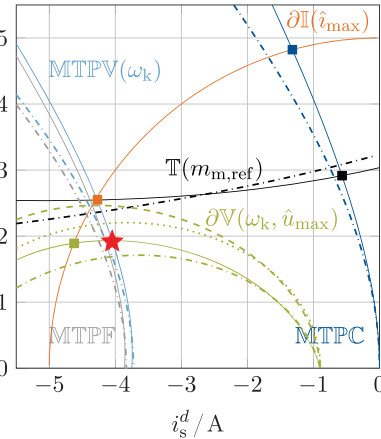
The derivation of the implicit form (23) is presented in Appendix A.2. Note that the presented derivation can also



(a)



(b)



(c)

Figure 4. Illustration of the impact of neglecting stator resistance (dashed line: $R_s = 0$), mutual inductance (dash-dotted: $L_m = 0$) or both (dotted: $R_s = L_m = 0$) on the different feedforward torque control strategies (a) MTPC, (b) FW and (c) MTPV from Figure 3: the three plots show voltage ellipse (—) $\partial V(\omega_k, \hat{u}_{\max})$, (---) $\partial V(\omega_k, \hat{u}_{\max}; R_s = 0)$, (-.-.-) $\partial V(\omega_k, \hat{u}_{\max}; L_m = 0)$, (.....) $\partial V(\omega_k, \hat{u}_{\max}; R_s = L_m = 0)$, maximum current circle (—) $\partial I(\hat{i}_{\max})$, MTPC hyperbola (—) MTPC, (-.-.-) MTPC($L_m = 0$), torque hyperbola (—) $T(m_{m,\text{ref}})$, (-.-.-) $T(m_{m,\text{ref}}; L_m = 0)$, MTPV hyperbola (—) MTPV(ω_k), (-.-.-) MTPV($\omega_k; L_m = 0$), MTPF hyperbola (—) MTPF, (-.-.-) MTPF($L_m = 0$) and optimal operation point (★), respectively.

be applied to obtain the implicit forms of the other operation strategies MC, FW, MTPV or MTPF.

Remark 4.1 (Explicit expression for the MTPC hyperbola): Depending on the parameters L_s^d , L_s^q and L_m , the hyperbola can be expressed explicitly as follows:

$$\text{MTPC}(i_s^d) = \begin{cases} \frac{2L_m i_s^d + \frac{\psi_{\text{pm}}^q}{2} \pm \sqrt{M}}{L_s^d - L_s^q} & \text{for } L_s^d \neq L_s^q \\ -(i_s^d = 0), & \text{for } L_s^d = L_s^q, \end{cases} \quad (25)$$

with $M := [(L_s^d - L_s^q)^2 + 4L_m^2](i_s^d)^2 + (2\psi_{\text{pm}}^q L_m + (L_s^d - L_s^q)\psi_{\text{pm}}^d)i_s^d + \frac{(\psi_{\text{pm}}^q)^2}{4}$. Obviously, (25) holds only for $i_s^d \leq 0$ and $L_s^q \geq L_s^d$. For $i_s^d > 0$ and/or $L_s^d = L_s^q$, another explicit expression has to be found. The implicit form (23)

with (24) holds in general (a significant advantage obviating the need of case studies). The mathematical derivation of the explicit expression of a general quadric is explained in Appendix A.3.

Remark 4.2 (MTPC versus MTPA): In most publications, the MTPC strategy is called MTPA. From a physical point of view, the use of physical quantities in the terminology (like torque and current) seems more appropriate than a mixture of quantity and unit (like torque and Ampere). Therefore, in this paper, the terminology MTPC will be adopted instead of MTPA (following the publications, Horlbeck & Hackl, 2016; Huber, Peters, & Böcker, 2015; Peters, Wallscheid, & Böcker, 2015).

4.2 Maximum current (MC)

To operate the machine at its current limit for increasing angular velocities, the MC strategy is used where the maximally feasible torque should be produced, i.e.

$$\begin{aligned} & \max_{\mathbf{i}_s^k \in \mathbb{S}} \text{sign}(m_{m,\text{ref}}) m_m(\mathbf{i}_s^k) \text{ with} \\ & \mathbb{S} := \partial \mathbb{I}(\hat{\mathbf{i}}_{\text{max}}) \cap \mathbb{V}(\omega_k, \hat{\mathbf{u}}_{\text{max}}). \end{aligned}$$

The optimal reference currents are obtained as the intersection points of the current circle $\partial \mathbb{I}(\hat{\mathbf{i}}_{\text{max}})$ and the voltage ellipse $\partial \mathbb{V}(\omega_k, \hat{\mathbf{u}}_{\text{max}})$. Hence, the reference current vectors are element of the following set:

$$\begin{aligned} \text{MC}(\omega_k, \hat{\mathbf{u}}_{\text{max}}, \hat{\mathbf{i}}_{\text{max}}) & \\ & := \partial \mathbb{I}(\hat{\mathbf{i}}_{\text{max}}) \cap \partial \mathbb{V}(\omega_k, \hat{\mathbf{u}}_{\text{max}}) \\ & = \left\{ \mathbf{i}_s^k \in \mathbb{R}^2 \mid (\mathbf{i}_s^k)^\top \mathbf{I}_2 \mathbf{i}_s^k - \hat{i}_{\text{max}}^2 = 0 \quad \wedge \right. \\ & \quad \left. (\mathbf{i}_s^k)^\top \mathbf{V}(\omega_k) \mathbf{i}_s^k + 2 \mathbf{v}(\omega_k)^\top \mathbf{i}_s^k + \nu(\omega_k, \hat{\mathbf{u}}_{\text{max}}) = 0 \right\} \end{aligned} \quad (26)$$

with \mathbf{V} , \mathbf{v} and ν as in (15). An algorithm to compute these intersection points *analytically* is presented in Appendix A.4.

4.3 Field weakening (FW)

For a feasible torque below rated machine torque and angular velocities higher than a certain feasible MTPC velocity, the machine is operated in FW. The optimisation problem for FW is identical to the optimisation problem for MTPC as in (22). Due to a smaller feasible set $\mathbb{S} := \mathbb{V}(\omega_k, \hat{\mathbf{u}}_{\text{max}}) \cap \mathbb{I}(\hat{\mathbf{i}}_{\text{max}})$, the optimal reference currents are obtained by the intersection of the (feasible) torque hyperbola $\mathbb{T}(m_{m,\text{ref}})$ and the voltage ellipse $\partial \mathbb{V}(\omega_k, \hat{\mathbf{u}}_{\text{max}})$, and hence the reference current vector is the element of the following set:

$$\begin{aligned} \text{FW}(m_{m,\text{ref}}, \omega_k, \hat{\mathbf{u}}_{\text{max}}) & \\ & := \mathbb{T}(m_{m,\text{ref}}) \cap \partial \mathbb{V}(\omega_k, \hat{\mathbf{u}}_{\text{max}}) \\ & = \left\{ \mathbf{i}_s^k \in \mathbb{R}^2 \mid (\mathbf{i}_s^k)^\top \mathbf{T} \mathbf{i}_s^k + 2 \mathbf{t}^\top \mathbf{i}_s^k + \tau(m_{m,\text{ref}}) = 0 \quad \wedge \right. \\ & \quad \left. (\mathbf{i}_s^k)^\top \mathbf{V}(\omega_k) \mathbf{i}_s^k + 2 \mathbf{v}(\omega_k)^\top \mathbf{i}_s^k + \nu(\omega_k, \hat{\mathbf{u}}_{\text{max}}) = 0 \right\} \end{aligned} \quad (27)$$

with \mathbf{T} , \mathbf{t} and $\tau(m_{m,\text{ref}})$ as in (9) and $\mathbf{V}(\omega_k)$, $\mathbf{v}(\omega_k)$ and $\nu(\omega_k, \hat{\mathbf{u}}_{\text{max}})$ as in (15). Again, the computation of the intersection points is based on the analytical algorithm presented in Appendix A.4.

4.4 Maximum torque per voltage (MTPV) hyperbola (considering R_s and L_m)

For high speeds and for torques higher than or equal to the speed-dependent MTPV cut-in torque $m_{m,\text{cut-in}}^{\text{MTPV}}$ (for details, see Section 5.1), the voltage constraint in (5) is critical and dominates the operation of the machine. Now, the operation strategy is MTPV. The corresponding MTPV optimisation problem is formulated as follows:

$$\begin{aligned} & \max_{\mathbf{i}_s^k \in \mathbb{S}} -\|\mathbf{u}_s^k(\mathbf{i}_s^k)\|^2 \\ & \text{s.t. } m_m(\mathbf{i}_s^k) = (\mathbf{i}_s^k)^\top \mathbf{T} \mathbf{i}_s^k + 2 \mathbf{t}^\top (\mathbf{i}_s^k) \stackrel{!}{=} m_{m,\text{ref}}, \end{aligned} \quad (28)$$

with $\mathbb{S} = \mathbb{V}(\omega_k, \hat{\mathbf{u}}_{\text{max}}) \cap \mathbb{I}(\hat{\mathbf{i}}_{\text{max}})$. Its solution, the MTPV hyperbola (see light blue line (—) in Figure 3), is parameterised by the electrical angular velocity ω_k and is implicitly given by the quadric

$$\begin{aligned} \text{MTPV}(\omega_k) & \\ & := \left\{ \mathbf{i}_s^k \in \mathbb{R}^2 \mid (\mathbf{i}_s^k)^\top \mathbf{M}_V(\omega_k) \mathbf{i}_s^k + 2 \mathbf{m}_V(\omega_k)^\top \mathbf{i}_s^k \right. \\ & \quad \left. + \mu_V(\omega_k) = 0 \right\} \end{aligned} \quad (29)$$

where

$$\begin{aligned} \mathbf{M}_V(\omega_k) & \\ & := \begin{bmatrix} m_V^{11}(\omega_k) & m_V^{12}(\omega_k) \\ m_V^{12}(\omega_k) & m_V^{22}(\omega_k) \end{bmatrix} = \mathbf{M}_V(\omega_k)^\top = \\ & = \frac{3}{2} n_p \begin{bmatrix} \omega_k^2 L_m^2 (L_s^d + L_s^q) & \frac{L_m}{2} (2R_s^2 + \omega_k^2 [(L_s^d)^2 \\ + \frac{L_s^d - L_s^q}{2} (R_s^2) + (L_s^q)^2 + 2L_m^2]) \\ \frac{L_m}{2} (2R_s^2 + \omega_k^2 [(L_s^d)^2 \\ + (L_s^q)^2 + 2L_m^2]) & \omega_k^2 L_m^2 (L_s^d + L_s^q) \\ & - \frac{L_s^d - L_s^q}{2} (R_s^2) \\ & + \omega_k^2 [(L_s^q)^2 + L_m^2]) \end{bmatrix}, \\ \mathbf{m}_V(\omega_k) & \\ & := \begin{pmatrix} m_V^1(\omega_k) \\ m_V^2(\omega_k) \end{pmatrix} = \begin{pmatrix} (R_s^2 + \omega_k^2 [2(L_s^d)^2 - L_s^q L_s^d + 3L_m^2]) \frac{\psi_{\text{pm}}^d}{4} \\ + \omega_k^2 L_m (L_s^d + L_s^q) \frac{\psi_{\text{pm}}^q}{2} \\ \omega_k^2 L_m (L_s^d + L_s^q) \frac{\psi_{\text{pm}}^d}{2} + (R_s^2 + \omega_k^2 [2(L_s^d)^2 \\ - L_s^q L_s^d + 3L_m^2]) \frac{\psi_{\text{pm}}^q}{4} \end{pmatrix} \text{ and} \\ \mu_V(\omega_k) & \\ & := \frac{3}{4} n_p \omega_k^2 \left[L_s^d (\psi_{\text{pm}}^d)^2 + 2L_m \psi_{\text{pm}}^d \psi_{\text{pm}}^q + L_s^q (\psi_{\text{pm}}^q)^2 \right] \\ & \stackrel{(2)}{=} \begin{cases} \frac{3}{4} n_p \omega_k^2 L_s^d \psi_{\text{pm}}^2, & \text{PMSM and PME-RSM,} \\ \frac{3}{4} n_p \omega_k^2 L_s^q \psi_{\text{pm}}^2, & \text{PMA-RSM, or} \\ 0, & \text{RSM.} \end{cases} \end{aligned} \quad (30)$$

Obviously, since $\mathbf{M}_V(\omega_k)$, $\mathbf{m}_V(\omega_k)$ and $\mu_V(\omega_k)$ all depend on the angular velocity ω_k , the MTPV hyperbola is moving in the (i_s^d, i_s^q) -plane (see thick light blue lines (—) in Figure 3(a–c)).

Remark 4.3 (Explicit expression for the MTPV hyperbola): The explicit solution of the MTPV hyperbola is given by (see Appendix A.3)

$$\begin{aligned} \text{MTPV}(i_s^d, \omega_k) &= -\frac{m_V^{12} i_s^d + m_V^2}{m_V^{22}} \\ &\pm \frac{\sqrt{(m_V^{12} i_s^d + m_V^2)^2 - m_V^{22} (m_V^{11} (i_s^d)^2 + 2m_V^1 i_s^d + \mu_V)}}{m_V^{22}}, \end{aligned} \quad (31)$$

where $m_V^{11} = m_V^{11}(\omega_k)$, $m_V^{12} = m_V^{12}(\omega_k)$, $m_V^{22} = m_V^{22}(\omega_k)$, $m_V^1 = m_V^1(\omega_k)$, $m_V^2 = m_V^2(\omega_k)$ and $\mu_V = \mu_V(\omega_k)$ are as in (30). Note that $m_V^{22}(0) = -\frac{L_s^d - L_s^q}{2} R_s^2 \neq 0$, and hence is non-zero for all ω_k and all $L_s^d \neq L_s^q$.

Remark 4.4 (MTPV hyperbola without stator resistance): Note that the MTPV hyperbola without stator resistance can be obtained from (30) by setting $R_s = 0$. This was already shown in Horlbeck and Hackl (2016).

4.5 Maximum torque per flux (MTPF) hyperbola (considering L_m)

For high speeds, an alternative to the MTPV strategy is the MTPF strategy. Nevertheless, it yields a reference current vector with larger magnitude than that obtained from MTPV. Hence, the MTPV strategy should be preferred (see also Remark 4.6). The MTPF optimisation problem can be formulated as follows:

$$\begin{aligned} \max_{i_s^k \in \mathbb{S}} & -\|\boldsymbol{\psi}_s^k(i_s^k)\|^2 \\ \text{s.t. } & m_m(i_s^k) = (i_s^k)^\top \mathbf{T} i_s^k + 2\mathbf{t}^\top (i_s^k) \stackrel{!}{=} m_{m,\text{ref}} \end{aligned} \quad (32)$$

with $\mathbb{S} := \mathbb{V}(\omega_k, \hat{u}_{\max}) \cap \mathbb{I}(\hat{i}_{\max})$. Its solution, the MTPF hyperbola (see gray line (—) in Figure 3), is implicitly given by the quadric

$$\text{MTPF} := \{i_s^k \in \mathbb{R}^2 \mid (i_s^k)^\top \mathbf{M}_F i_s^k + 2\mathbf{m}_F^\top i_s^k + \mu_F = 0\}, \quad (33)$$

which does *not* depend on the angular velocity ω_k (in contrast to the MTPV hyperbola (29)), since

$$\begin{aligned} \mathbf{M}_F &:= \begin{bmatrix} m_F^{11} & m_F^{12} \\ m_F^{12} & m_F^{22} \end{bmatrix} = \mathbf{M}_F^\top = \\ &= \frac{3}{2} n_p \begin{bmatrix} \frac{L_s^d - L_s^q}{2} ((L_s^d)^2 + L_m^2) + L_m^2 (L_s^d + L_s^q) + (L_s^q)^2 + 2L_m^2, & \frac{L_m}{2} ((L_s^d)^2 \\ & + (L_s^q)^2 + 2L_m^2), \end{bmatrix}, \\ \mathbf{m}_F &:= \begin{pmatrix} m_F^1 \\ m_F^2 \end{pmatrix} \\ &= \frac{3}{2} n_p \begin{pmatrix} \left(2(L_s^d)^2 - L_s^d L_s^q + 3L_m^2 \right) \frac{\psi_{\text{pm}}^d}{4} \\ + L_m (L_s^d + L_s^q) \frac{\psi_{\text{pm}}^q}{2} \\ L_m (L_s^d + L_s^q) \frac{\psi_{\text{pm}}^d}{2} \\ + \left(2(L_s^q)^2 - L_s^d L_s^q + 3L_m^2 \right) \frac{\psi_{\text{pm}}^q}{4} \end{pmatrix} \text{ and} \\ \mu_F &:= \frac{3}{4} n_p \left[L_s^d (\psi_{\text{pm}}^d)^2 + 2L_m \psi_{\text{pm}}^d \psi_{\text{pm}}^q + L_s^q (\psi_{\text{pm}}^q)^2 \right] \\ &\stackrel{(2)}{=} \begin{cases} \frac{3}{4} n_p L_s^d (\psi_{\text{pm}}^d)^2, & \text{PMSM and PME-RSM,} \\ \frac{3}{4} n_p L_s^q (\psi_{\text{pm}}^q)^2, & \text{for PMA-RSM,} \\ 0, & \text{RSM,} \end{cases} \end{aligned} \quad (34)$$

do *not* depend on the electrical angular velocity ω_k , respectively.

Remark 4.5 (Explicit expression for the MTPF hyperbola): The explicit solution of the MTPF hyperbola is given by (see again Appendix A.3)

$$\begin{aligned} \text{MTPF}(i_s^d) &= -\frac{m_F^{12} i_s^d + m_F^2}{m_F^{22}} \\ &\pm \frac{\sqrt{(m_F^{12} i_s^d + m_F^2)^2 - m_F^{22} (m_F^{11} (i_s^d)^2 + 2m_F^1 i_s^d + \mu_F)}}{m_F^{22}}, \end{aligned} \quad (35)$$

where m_F^{11} , m_F^{12} , m_F^{22} , m_F^1 , m_F^2 and μ_F are as in (34). Note that $m_F^{22} = \frac{3}{2} n_p \left[-\frac{L_s^d - L_s^q}{2} ((L_s^q)^2 + L_m^2) + L_m^2 (L_s^d + L_s^q) \right] \neq 0$.

Remark 4.6 (Convergence of the MTPV hyperbola to the MTPF hyperbola): For very large electrical angular velocities, i.e. $|\omega_k| \gg 1$, or very small stator resistances, i.e. $R_s \ll 1 \Omega$, the MTPV hyperbola converges to the shape of the MTPF hyperbola, since, either for $\omega_k \rightarrow \infty$ or for

Table 1. Analytical solutions of the optimal current reference vectors for all operation strategies.

Strategy	Current reference vector	Algorithm used
MTPC	$\mathbf{i}_{s,\text{ref}}^{k,\text{MTPC}}(\lambda^*) \stackrel{(A14)}{:=} -[\lambda^* \mathbf{T} - \mathbf{I}_2]^{-1} \lambda^* \mathbf{t}$	See Appendix A.1
or	$\mathbf{i}_{s,\text{ref}}^{k,\text{MTPC}}(\gamma^*) \stackrel{(A32)}{:=} -2[\mathbf{D} - \gamma^* \mathbf{J}]^{-1} \mathbf{d}$	See Appendix A.4 (case (ii) for $\text{MTPC} \cap \mathbb{T}(m_{m,\text{ref}})$)
for RSM	$\mathbf{i}_{s,\text{ref}}^{k,\text{MTPC}}(\gamma^*) \stackrel{(A32)}{:=} -2[\mathbf{D} - \gamma^* \mathbf{J}]^{-1} \mathbf{d} + \mathbf{x}_s$	See Appendix A.4 (case (iii) for $\text{MTPC} \cap \mathbb{T}(m_{m,\text{ref}})$)
MC	$\mathbf{i}_{s,\text{ref}}^{k,\text{MC}}(\gamma^*) \stackrel{(A32)}{:=} -2[\mathbf{D} - \gamma^* \mathbf{J}]^{-1} \mathbf{d}$	See Appendix A.4 (case (i) for $\partial \mathbb{I}(\hat{u}_{\max}) \cap \partial \mathbb{V}(\omega_k, \hat{u}_{\max})$)
for RSM	$\mathbf{i}_{s,\text{ref}}^{k,\text{MC}}(\gamma^*) \stackrel{(A32)}{:=} -2[\mathbf{D} - \gamma^* \mathbf{J}]^{-1} \mathbf{d} + \mathbf{x}_s$	See Appendix A.4 (case (iii) for $\partial \mathbb{I}(\hat{u}_{\max}) \cap \partial \mathbb{V}(\omega_k, \hat{u}_{\max})$)
FW	$\mathbf{i}_{s,\text{ref}}^{k,\text{FW}}(\gamma^*) \stackrel{(A32)}{:=} -2[\mathbf{D} - \gamma^* \mathbf{J}]^{-1} \mathbf{d}$	See Appendix A.4 (case (i) for $\partial \mathbb{T}(m_{m,\text{ref}}) \cap \partial \mathbb{V}(\omega_k, \hat{u}_{\max})$)
for RSM	$\mathbf{i}_{s,\text{ref}}^{k,\text{FW}}(\gamma^*) \stackrel{(A32)}{:=} -2[\mathbf{D} - \gamma^* \mathbf{J}]^{-1} \mathbf{d} + \mathbf{x}_s$	See Appendix A.4 (case (iii) for $\partial \mathbb{T}(m_{m,\text{ref}}) \cap \partial \mathbb{V}(\omega_k, \hat{u}_{\max})$)
MTPF	$\mathbf{i}_{s,\text{ref}}^{k,\text{MTPF}}(\gamma^*) \stackrel{(A32)}{:=} -2[\mathbf{D} - \gamma^* \mathbf{J}]^{-1} \mathbf{d}$	See Appendix A.4 (case (i) for $\text{MTPF} \cap \partial \mathbb{V}(\omega_k, \hat{u}_{\max})$)
for RSM	$\mathbf{i}_{s,\text{ref}}^{k,\text{MTPF}}(\gamma^*) \stackrel{(A32)}{:=} -2[\mathbf{D} - \gamma^* \mathbf{J}]^{-1} \mathbf{d} + \mathbf{x}_s$	See Appendix A.4 (case (iii) for $\text{MTPF} \cap \partial \mathbb{V}(\omega_k, \hat{u}_{\max})$)
MTPV	$\mathbf{i}_{s,\text{ref}}^{k,\text{MTPV}}(\gamma^*) \stackrel{(A32)}{:=} -2[\mathbf{D} - \gamma^* \mathbf{J}]^{-1} \mathbf{d}$	See Appendix A.4 (case (i) for $\text{MTPV}(\omega_k) \cap \partial \mathbb{V}(\omega_k, \hat{u}_{\max})$)
for RSM	$\mathbf{i}_{s,\text{ref}}^{k,\text{MTPV}}(\gamma^*) \stackrel{(A32)}{:=} -2[\mathbf{D} - \gamma^* \mathbf{J}]^{-1} \mathbf{d} + \mathbf{x}_s$	See Appendix A.4 (case (iii) for $\text{MTPV}(\omega_k) \cap \partial \mathbb{V}(\omega_k, \hat{u}_{\max})$)

$R_s = 0$, the following holds:

$$\begin{aligned} & (\mathbf{i}_s^k)^\top \mathbf{M}_F \mathbf{i}_s^k + 2 \mathbf{m}_F^\top \mathbf{i}_s^k + \mu_F = 0 \\ & = \begin{cases} \lim_{\omega_k \rightarrow \infty} (\mathbf{i}_s^k)^\top \frac{\mathbf{M}_V(\omega_k)}{\omega_k^2} \mathbf{i}_s^k \\ \quad + 2 \frac{\mathbf{m}_V(\omega_k)^\top}{\omega_k^2} \mathbf{i}_s^k + \frac{\mu_V(\omega_k)}{\omega_k^2}, & R_s \neq 0 \\ (\mathbf{i}_s^k)^\top \frac{\mathbf{M}_V(\omega_k)}{\omega_k^2} \mathbf{i}_s^k + 2 \frac{\mathbf{m}_V(\omega_k)^\top}{\omega_k^2} \mathbf{i}_s^k \\ \quad + \frac{\mu_V(\omega_k)}{\omega_k^2}, & R_s = 0. \end{cases} \end{aligned}$$

Concluding, *only* for very large speeds or very small values of the stator resistance, both strategies are similar. In general, MTPF and MTPV hyperbola are *different* solutions to different optimisation problems and give different optimal reference currents (see [Figure 3\(c\)](#)): the MTPV hyperbola is approaching the MTPF hyperbola for increasing speeds; but the hyperbolas do *not* coincide).

4.6 Analytical solutions of the optimal reference current vectors for MTPC, MC, FW, MTPV and MTPF

As soon as the implicit expressions (quadrics)

- (i) for the constraints (i.e. voltage ellipse $\mathbb{V}(\hat{u}_{\max}, \omega_k)$, current circle $\mathbb{I}(\hat{u}_{\max})$, and torque hyperbola $\mathbb{T}(m_{m,\text{ref}})$) and

- (ii) for the operation strategies MTPC, MTPV, and MTPF (i.e. MTPC, $\text{MTPV}(\omega_k)$ and MTPF hyperbola, respectively)

are derived, the optimal reference currents $\mathbf{i}_{s,\text{ref}}^k = \mathbf{i}_{s,\text{ref}}^{k,X}$ for each operation strategy $X \in \{\text{MTPC}, \text{MC}, \text{FW}, \text{MTPV}, \text{MTPF}\}$ are obtained by intersecting the respective quadrics (following the general approach presented in [Appendix A.4](#)).

In [Table 1](#), for each operation strategy, the analytical expression for the optimal current reference vector and the used computation method (algorithm) are listed in compact form. In all cases, λ^* and γ^* are the optimal Lagrangian multipliers which represent one of the (real) roots of the polynomial [\(A9\)](#) and [\(A30\)](#), respectively. The four roots can be computed analytically by the algorithm presented in [Appendix A.1.3](#) (Euler's solution; Rees, 1922).

Remark 4.7 (Alternative computation of optimal reference currents for MTPC):

Note that, alternatively, by using the algorithm discussed in [Appendix A.4](#), the optimal current reference vectors for MTPC can also be obtained by computing the intersection points of torque hyperbola [\(12\)](#) and MTPC hyperbola [\(23\)](#) (see also [Table 1](#)).

Remark 4.8 (Optimal reference currents for RSMs): The analytical solutions for RSMs can be computed in a similar way as shown in Table 1; however, for RSMs, all quadrics simplify due to the missing permanent magnet, i.e. $\psi_{\text{pm}}^d = \psi_{\text{pm}}^q = 0$. The vectors $\mathbf{t} = \mathbf{v}(\omega_k) = \mathbf{f} = \mathbf{m}_C = \mathbf{m}_V(\omega_k) = \mathbf{m}_F = \mathbf{0}_2$ and scalars $\phi = \mu_V(\omega_k) = \mu_F = 0$ of torque hyperbola (12), voltage ellipse (17), flux norm (20), MTPC hyperbola (23), MTPV hyperbola (29) and MTPF hyperbola (33) become zero (see also (9), (15), (21), (24), (30) and (34)), respectively. Therefore, instead of applying case (i) of Appendix A.4, case (iii) of Appendix A.4 must be considered for the computation of the intersection points of the respective quadrics (see also Table 1).

4.7 Graphical illustration

In Figure 3, for a small 400 W IPMSM with the following parameters:

$$\left. \begin{aligned} R_s &= 20 \, \Omega, L_s^d = 6 \cdot 10^{-2} \, \text{H}, \\ L_s^q &= 8 \cdot 10^{-2} \, \text{H}, L_m = 0.5 \cdot 10^{-3} \, \text{H}, \\ \psi_{\text{pm}}^k &= (\psi_{\text{pm}}, 0)^\top = (0.23 \, \text{Wb}, 0)^\top \text{ and } n_p = 3, \end{aligned} \right\} \quad (36)$$

three different optimal feedforward torque control strategies are illustrated for the positive reference torque $m_{m,\text{ref}} = 3.35 \, \text{N m}$, the voltage limit $\hat{u}_{\text{max}} = 600 \, \text{V}$ and the current limit $\hat{i}_{\text{max}} = 5 \, \text{A}$. The illustrated optimal operation strategies are MTPC in Figure 3(a), FW in Figure 3(b) and MTPV in Figure 3(c). The respective optimal operation point, with its (optimal) reference current vector $\mathbf{i}_{s,\text{ref}}^k = (i_{s,\text{ref}}^d, i_{s,\text{ref}}^q)^\top$, is marked by \star and corresponds to the intersection of (a) $\text{MTPC} \cap \mathbb{T}(m_{m,\text{ref}})$ for MTPC in Figure 3(a), (b) $\partial\mathbb{V}(\omega_k, \hat{u}_{\text{max}}) \cap \mathbb{T}(m_{m,\text{ref}})$ for FW in Figure 3(b), and (c) $\text{MTPV} \cap \partial\mathbb{V}(\omega_k, \hat{u}_{\text{max}})$ for MTPV in Figure 3(c).

For increasing electrical angular velocities $\omega_k \in \{1, 2, 3\}\omega_{k,\text{nom}}$ (where $\omega_{k,\text{nom}}$ is the nominal electrical angular velocity, see also Section 5.1), the MTPV hyperbola is approaching the MTPF hyperbola (recall Remark 4.6) and the voltage ellipse is shrinking; whereas the current circle, MTPC hyperbola, torque hyperbola and MTPF hyperbola are independent of the angular velocity and hence do *not* change in the three plots. The blue square represents the intersection point of the MTPC hyperbola with the current circle and gives the nominal current vector $\mathbf{i}_{s,\text{nom}}^k$ producing the nominal torque $m_{m,\text{nom}}(\mathbf{i}_{s,\text{nom}}^k)$. The orange square highlights the intersection of current circle and torque hyperbola (in the second quadrant) and represents the maximally

feasible current and maximally feasible torque for higher angular velocities.

Figure 4(a–c) illustrates the impact of neglecting (i) stator resistance (i.e. $R_s = 0$: dashed line), (ii) mutual inductance (i.e. $L_m = 0$: dash-dotted line) or (iii) both (i.e. $R_s = L_m = 0$: dotted line) on the shape of MTPC, MTPV, MTPF, and torque hyperbolas and the voltage ellipse. The feedforward torque control strategies and optimal operation points (marked by \star) are identical to those shown in Figure 3. It is easy to see that neglecting stator resistance, mutual inductance or both would lead to completely different (and wrong) intersection points, and hence *not* optimal operation points with *reduced efficiency*. For example, the impact of neglecting stator resistance, mutual inductance or both on the shape, size and orientation of the voltage ellipse is obvious. Concluding, for optimal operation of an SM, both parameters must *not* be neglected.

In Figures 3 and 4, the intersection points of (i) current circle and MTPC hyperbola, (ii) current circle and MTPV hyperbola, (iii) current circle and voltage ellipse, and (iv) torque and MTPC hyperbola are highlighted by the following coloured squares (i) \blacksquare , (ii) \blacksquare , (iii) \blacksquare and (iv) \blacksquare , respectively. These intersection points will be crucial for the operation management.

5. Operation management (see Figure 5)

Depending on the electrical angular velocity $\omega_k = n_p \omega_m$, reference torque $m_{m,\text{ref}}$, maximal current \hat{i}_{max} and voltage \hat{u}_{max} (and the machine parameters), different operation strategies must be selected online. The flowchart depicted in Figure 5(a) illustrates the procedure to determine the optimal reference current vector $\mathbf{i}_{s,\text{ref}}^k$ regarding the defined control objectives such as MTPC, MC, FW and MTPV. Figure 5(b,c) show the different operation strategies in the machine map (torque over speed) and in the current locus, respectively. The overall goal is to produce the reference torque with the minimum current magnitude to increase the machine efficiency. However, if the reference torque is not feasible (due to physical constraints), a deviation from the reference torque is allowed in the sense that the *maximally available (feasible)* torque is produced in the electrical machine. This allows to operate the machine over the whole speed range at the cost of efficiency but beyond nominal speed.

5.1 Operation management parameters

Before the operation management will be explained in more detail in Section 5.2, the following five crucial *operation management parameters* (see Figure 5) are

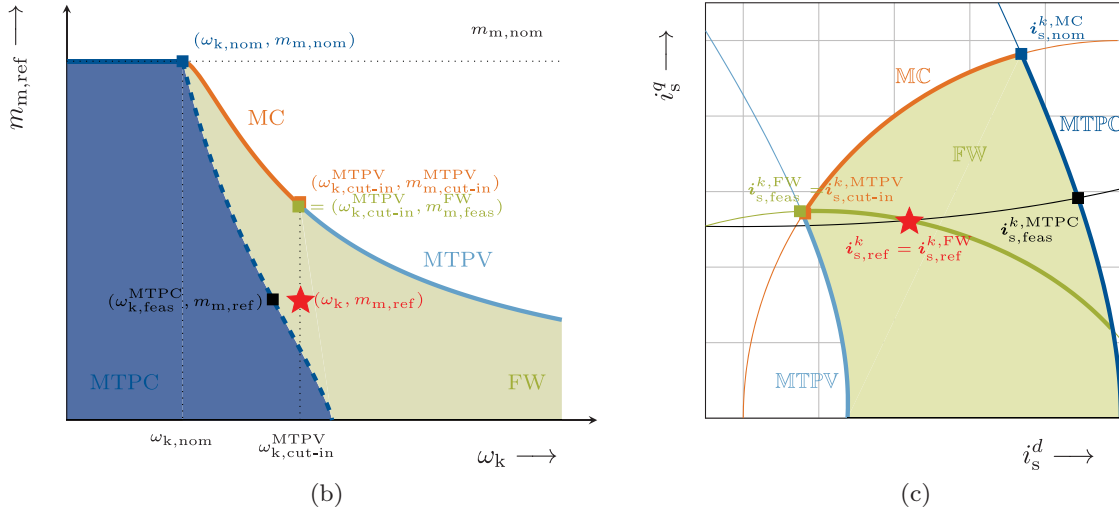
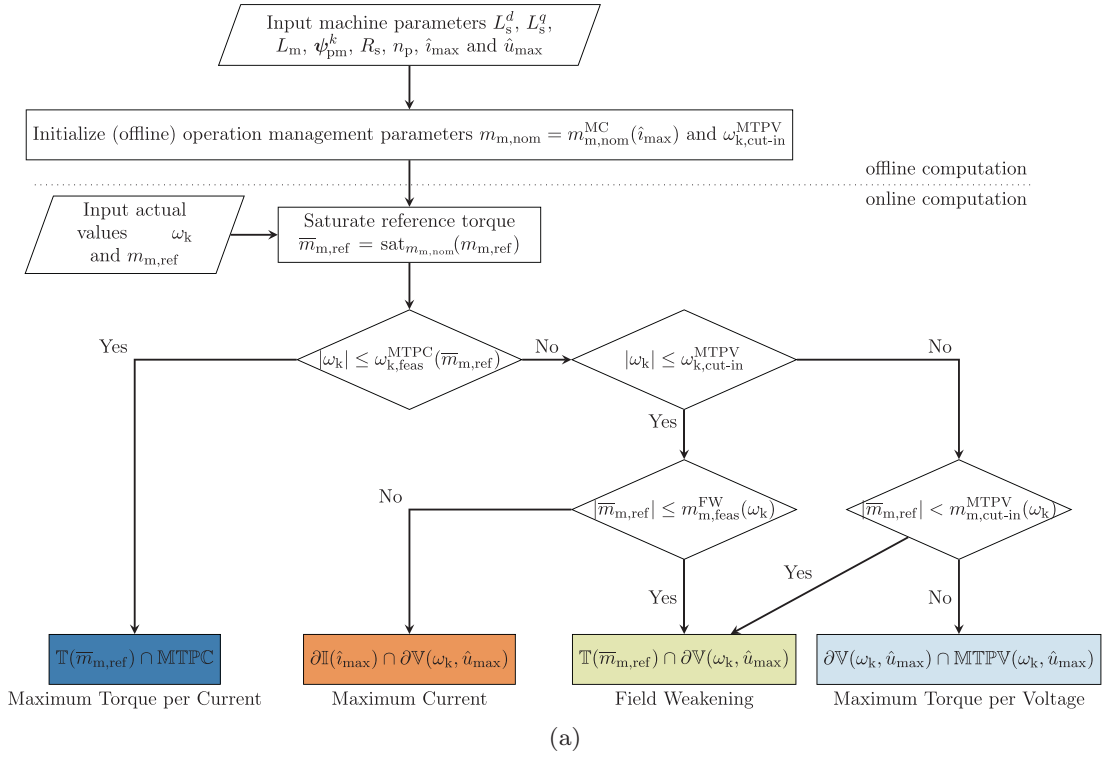


Figure 5. Illustration of operation management: (a) Flow chart illustrating the decision tree for the selection of the optimal operation strategy, (b) machine map with threshold speed $\omega_{k,\text{feas}}^{\text{MTPC}}(m_{m,\text{ref}})$ (see thick dashed line) for $\omega_k = \omega_{k,\text{cut-in}}^{\text{MTPV}}$ and $m_{m,\text{ref}} \leq m_{m,\text{feas}}^{\text{FW}}$, and (c) current locus for $\omega_k = \omega_{k,\text{cut-in}}^{\text{MTPV}}$ and $m_{m,\text{ref}} \leq m_{m,\text{feas}}^{\text{FW}}$.

introduced which allow to select the actually optimal operation strategy online:

- $m_{m,\text{nom}} = m_{m,\text{nom}}^{\text{MC}}(i_{s,\text{nom}}^k)$: The *nominal machine torque* which cannot be exceeded permanently due to the current limit \hat{i}_{max} . The nominal torque is a result of the nominal current vector $i_{s,\text{nom}}^k = i_{s,\text{nom}}^{k,\text{MC}}(\hat{i}_{\text{max}})$ which represents the intersection point of current circle and MTPC hyperbola (see blue square (■) in Figure 5(c)).

- $\omega_{k,\text{feas}}^{\text{MTPC}}(m_{m,\text{ref}})$: The *maximally feasible MTPC angular velocity* for a given reference torque $m_{m,\text{ref}}$ during MTPC operation. An operation in MTPC mode is only feasible below this speed limit. Note that $\omega_{k,\text{feas}}^{\text{MTPC}}(m_{m,\text{ref}})$ is a function of the actually commanded reference torque $m_{m,\text{ref}}$, hence its value will change for varying reference torques. For example, for smaller reference torques, MTPC is feasible for higher speeds than for larger reference torques (see dashed blue line (---) in Figure 5(b)).

- $m_{m,feas}^{FW}(\omega_k)$: The *maximally feasible FW torque* during FW operation which varies with the electrical angular velocity ω_k . Only for torques below this limit an operation in FW mode is feasible.
- $\omega_{k,cut-in}^{MTPV} = \omega_{k,cut-in}^{MTPV}(\hat{i}_{max}, \hat{u}_{max})$: the *constant MTPV cut-in angular velocity* which depends on (constant) current \hat{i}_{max} and voltage \hat{u}_{max} limit. For actual angular velocities above this limit and non-feasible (too high) torques (see the next item), solely an operation in MTPV mode is admissible (see Figure 5(b)).
- $m_{m,cut-in}^{MTPV}(\omega_k)$: The *MTPV cut-in torque* which varies with the actual angular velocity ω_k . For speeds above $\omega_{k,cut-in}^{MTPV}$ and for reference torques higher than $m_{m,cut-in}^{MTPV}(\omega_k)$, the machine must be operated in MTPV mode.

The parameters $m_{m,nom}$ and $\omega_{k,cut-in}^{MTPV}$ are *constant* (if \hat{i}_{max} and \hat{u}_{max} are constant) and, therefore, can be computed *offline*. The remaining three parameters $\omega_{k,feas}^{MTPC}(m_{m,ref})$, $m_{m,feas}^{FW}(\omega_k)$ and $m_{m,cut-in}^{MTPV}(\omega_k)$ do vary with the reference torque $m_{m,ref}$ or the angular velocity ω_k and hence are (usually) *not* constant during operation. These parameters have to be computed *online*.

5.1.1 Offline computation of the nominal machine torque $m_{m,nom}$ (based on the current constraint \hat{i}_{max})
The nominal (or maximal) machine torque $m_{m,nom} = m_{m,nom}^{MC}(\hat{i}_{max})$ can be produced for the maximally admissible (nominal) current vector $\mathbf{i}_{s,nom}^k$ on the current circle during MTPC operation. The nominal MTPC current vector $\mathbf{i}_{s,nom}^k$ is obtained at the intersection of MTPC hyperbola (23) and current circle (19), i.e. $\mathbf{i}_{s,nom}^k \in \text{MTPC} \cap \partial\mathbb{I}(\hat{i}_{max})$. The intersection point(s) $\mathbf{i}_{s,nom}^{k,MC}(\hat{i}_{max})$ can be computed *analytically* by invoking the algorithm presented in Appendix A.4 (see also Table 1). The nominal current $i_{s,nom}^k = i_{s,nom}^{k,MC}(\hat{i}_{max})$ is the intersection point in the second quadrant of the current loci (see ■ in Figure 5(b) or 5(c)). Inserting $\mathbf{i}_{s,nom}^k$ into the machine torque (3) yields the nominal torque defined by

$$\begin{aligned} m_{m,nom} &:= m_{m,nom}^{MC}(\hat{i}_{max}) \stackrel{(3)}{=} (\mathbf{i}_{s,nom}^k)^\top \mathbf{T} \mathbf{i}_{s,nom}^k + 2t^\top \mathbf{i}_{s,nom}^k \\ &= \frac{3}{2} n_p (\mathbf{i}_{s,nom}^k)^\top \mathbf{J} (\mathbf{L}_s^k \mathbf{i}_{s,nom}^k + \boldsymbol{\psi}_{pm}^k). \end{aligned} \quad (37)$$

Note that the nominal torque $m_{m,nom}$ can be exceeded temporarily by increasing \hat{i}_{max} for a short period of time.

Remark 5.1 (Computation of the nominal electrical angular velocity $\omega_{k,nom}$): In this paper, the nominal (or rated) angular velocity $\omega_{k,nom}$ is defined as the angular velocity where the voltage ellipse (see green line (—)) in Figure 5(c) intersects with the current circle (see orange line (—)) and the MTPC hyperbola (see blue

line (—)). Rewriting the voltage ellipse (17) as a function of ω_k (considering \mathbf{i}_s^k and \hat{u}_{max} as parameters) leads to the following quadratic polynomial:

$$Q_{\partial\mathbb{V}}(\mathbf{i}_s^k, \omega_k, \hat{u}_{max}) \stackrel{(17)}{=} \delta_2(\mathbf{i}_s^k) \omega_k^2 + \delta_1(\mathbf{i}_s^k) \omega_k + \delta_0(\mathbf{i}_s^k, \hat{u}_{max}) = 0 \quad (38)$$

with coefficients (depending on i_s^d, i_s^q and \hat{u}_{max})

$$\left. \begin{aligned} \delta_2(\mathbf{i}_s^k) &:= 2 \left[i_s^d (L_m \psi_{pm}^q + L_s^d \psi_{pm}^d) + i_s^q (L_m \psi_{pm}^d + L_s^q \psi_{pm}^q) \right] + i_s^d \left[i_s^q (L_m L_s^d + L_m L_s^q) + i_s^d (L_m^2 + (L_s^d)^2) \right] \\ &\quad + i_s^q \left[i_s^d (L_m L_s^d + L_m L_s^q) + i_s^q (L_m^2 + (L_s^q)^2) \right] + (\psi_{pm}^d)^2 + (\psi_{pm}^q)^2 \\ \delta_1(\mathbf{i}_s^k) &:= i_s^q \left[2L_m R_s i_s^q + R_s i_s^d (L_s^d - L_s^q) \right] - i_s^d \left[2L_m R_s i_s^d - R_s i_s^q (L_s^d - L_s^q) \right] \\ &\quad - 2R_s (i_s^d \psi_{pm}^q - i_s^q \psi_{pm}^d) \\ \delta_0(\mathbf{i}_s^k, \hat{u}_{max}) &:= R_s^2 (i_s^d)^2 + R_s^2 (i_s^q)^2 - \hat{u}_{max}^2. \end{aligned} \right\} \quad (39)$$

Inserting the nominal MTPC current vector $\mathbf{i}_s^k = \mathbf{i}_{s,nom}^k$ into (38) allows to compute the *nominal electrical angular velocity* $\omega_{k,nom}$ and the *nominal mechanical angular velocity* $\omega_{m,nom} = \frac{1}{n_p} \omega_{k,nom}$ as follows:

$$\begin{aligned} \omega_{k,nom} &:= n_p \omega_{m,nom} := \frac{\delta_1(\mathbf{i}_{s,nom}^k)}{2\delta_2(\mathbf{i}_{s,nom}^k)} \\ &\times \left(1 + \sqrt{1 - 4 \frac{\delta_0(\mathbf{i}_{s,nom}^k, \hat{u}_{max}) \delta_2(\mathbf{i}_{s,nom}^k)}{\delta_1(\mathbf{i}_{s,nom}^k)^2}} \right). \end{aligned} \quad (40)$$

5.1.2 Online computation (only if necessary) of the maximally feasible angular velocity $\omega_{k,feas}^{MTPC}(m_{m,ref})$ during MTPC operation

For a given reference torque $m_{m,ref}$ (assuming it is not exceeding the nominal torque), there exists an intersection point $\mathbf{i}_{s,feas}^{k,MTPC}(m_{m,ref})$ (in the second quadrant, see black square ■ in Figure 5(c)) of torque and MTPC hyperbola, i.e. $\mathbf{i}_{s,feas}^{k,MTPC}(m_{m,ref}) \in \text{MTPC} \cap \mathbb{T}(m_{m,ref})$. The intersection point(s) of the two quadrics can be computed analytically by using the algorithm presented in Appendix A.4. Inserting $\mathbf{i}_s^k = \mathbf{i}_{s,feas}^{k,MTPC}(m_{m,ref})$ into (38) and solving for ω_k yields the maximally feasible MTPC angular velocity (similar to (40)),

$$\begin{aligned} \omega_{k,feas}^{MTPC}(m_{m,ref}) &:= \frac{\delta_1(\mathbf{i}_{s,feas}^{k,MTPC}(m_{m,ref}))}{2\delta_2(\mathbf{i}_{s,feas}^{k,MTPC}(m_{m,ref}))} \\ &\times \left(1 + \sqrt{1 - 4 \frac{\delta_0(\mathbf{i}_{s,feas}^{k,MTPC}(m_{m,ref}), \hat{u}_{max}) \delta_2(\mathbf{i}_{s,feas}^{k,MTPC}(m_{m,ref}))}{\delta_1(\mathbf{i}_{s,feas}^{k,MTPC}(m_{m,ref}))^2}} \right). \end{aligned} \quad (41)$$

5.1.3 Offline computation of the (constant) MTPV cut-in angular velocity $\omega_{k,\text{cut-in}}^{\text{MTPV}} = \omega_{k,\text{cut-in}}^{\text{MTPV}}(\hat{i}_{\max}, \hat{u}_{\max})$

The MTPV cut-in speed $\omega_{k,\text{cut-in}}^{\text{MTPV}}$ defines the speed at which the current trajectory diverts from the current circle $\partial\mathbb{I}(\hat{i}_{\max})$ and starts moving on the MTPV hyperbola for maximum torque output. Mathematically, this point is described by the intersection of the three quadrics current circle, voltage ellipse and MTPV hyperbola, i.e. $\partial\mathbb{I}(\hat{i}_{\max}) \cap \text{MTPV}(\omega_k) \cap \partial\mathbb{V}(\omega_k, \hat{u}_{\max})$. All three quadrics are functions of the currents i_s^k and, the latter two, of the angular velocity ω_k additionally. This makes the problem solvable, since the given three equations and three unknowns can be resolved. However, to find the solution, the roots of a 16th-order polynomial must be found (see algorithm below), and hence $\omega_{k,\text{cut-in}}^{\text{MTPV}}$ is the only parameter which must be computed *numerically* (but offline). The procedure to obtain $\omega_{k,\text{cut-in}}^{\text{MTPV}}$ is as follows:

- (i) Rewrite the current circle $\partial\mathbb{I}(\hat{i}_{\max})$ as explicit function of one current component, e.g. $i_s^d = \sqrt{i_{\max}^2 - (i_s^q)^2}$.
- (ii) Insert this component into the voltage ellipse (17) and the MTPV hyperbola (29) to obtain two functions with the two unknowns ω_k and i_s^q .
- (iii) Rewrite these two functions as second-order polynomials in ω_k , i.e. $p_1 := a_2(i_s^d)\omega_k^2 + a_1(i_s^d)\omega_k + a_0(i_s^d)$ and $p_2 := b_2(i_s^d)\omega_k^2 + b_1(i_s^d)\omega_k + b_0(i_s^d)$ where the coefficients a_2, a_1, a_0 and b_2, b_1, b_0 depend on i_s^d , respectively.
- (iv) Define the *Sylvester matrix*

$$\mathbf{S}(i_s^d) := \begin{bmatrix} a_2(i_s^d) & a_1(i_s^d) & a_0(i_s^d) & 0 \\ 0 & a_2(i_s^d) & a_1(i_s^d) & a_0(i_s^d) \\ b_2(i_s^d) & b_1(i_s^d) & b_0(i_s^d) & 0 \\ 0 & b_2(i_s^d) & b_1(i_s^d) & b_0(i_s^d) \end{bmatrix}$$

and compute its *resultant* $\mathfrak{R}_S(i_s^d) := \det(\mathbf{S}(i_s^d))$ which is a 16th-order polynomial (see Zippel, 2012, pp. 141–146).

- (v) Solve $\mathfrak{R}_S(i_s^d) = 0$ numerically for i_s^d and insert the solution(s) into the current circle (19) to obtain values for i_s^q .
- (vi) Calculate the solution candidates for $\omega_{k,\text{cut-in}}^{\text{MTPV}}$ by inserting both currents into either the voltage ellipse (17) or the MTPV hyperbola (29) and choose the one with the smallest positive value.

5.1.4 Online computation (only if necessary) of the maximally feasible torque $m_{m,\text{feas}}^{\text{FW}}(\omega_k)$ during FW operation

For angular velocities higher than the feasible MTPC angular velocity, i.e. $|\omega_k| > \omega_{k,\text{feas}}^{\text{MTPC}}(m_{m,\text{ref}})$, and reference

torques smaller than the maximally feasible FW torque $m_{m,\text{feas}}^{\text{FW}}(\omega_k)$, i.e. $|m_{m,\text{ref}}| \leq m_{m,\text{feas}}^{\text{FW}}(\omega_k)$, FW is the optimal operation strategy of the electrical machine. For given ω_k , the current vector $i_{s,\text{feas}}^{k,\text{FW}}(\omega_k)$ (in the second quadrant, see green square ■ in Figure 5(c)) which represents the intersection of current circle and voltage ellipse, i.e. $\partial\mathbb{I}(\hat{i}_{\max}) \cap \partial\mathbb{V}(\omega_k, \hat{u}_{\max})$, is obtained *analytically* by invoking the algorithm in Appendix A.4. Inserting this current vector into the torque equation (3) gives the maximally feasible FW torque

$$m_{m,\text{feas}}^{\text{FW}}(\omega_k) \stackrel{(3)}{:=} \frac{3}{2} n_p (i_{s,\text{feas}}^{k,\text{FW}}(\omega_k))^\top \mathbf{J} (\mathbf{L}_s^k i_{s,\text{feas}}^{k,\text{FW}}(\omega_k) + \psi_{\text{pm}}^k), \quad (42)$$

which clearly varies with the actual angular velocity ω_k .

5.1.5 Online computation (only if necessary) of the MTPV cut-in torque $m_{m,\text{cut-in}}^{\text{MTPV}}(\omega_k)$ for MTPV operation

For angular velocities higher than the MTPV cut-in speed, i.e. $|\omega_k| > \omega_{k,\text{cut-in}}^{\text{MTPV}}$ and reference torques higher than the MTPV cut-in torque $m_{m,\text{cut-in}}^{\text{MTPV}}(\omega_k)$, i.e. $|m_{m,\text{ref}}| \geq m_{m,\text{cut-in}}^{\text{MTPV}}(\omega_k)$, the electrical machine must be operated in MTPV mode. For given ω_k , the intersection point $i_{s,\text{cut-in}}^{k,\text{MTPV}}(\omega_k)$ (in the second quadrant, see orange square ■ in Figure 5(c)) of voltage ellipse and MTPV hyperbola, i.e. $\partial\mathbb{V}(\omega_k, \hat{u}_{\max}) \cap \text{MTPV}(\omega_k)$, can be computed *analytically* with the help of the algorithm presented in Appendix A.4. Inserting the solution $i_{s,\text{cut-in}}^{k,\text{MTPV}}$ into the torque equation (3) gives the MTPV cut-in torque

$$m_{m,\text{cut-in}}^{\text{MTPV}}(\omega_k) \stackrel{(3)}{:=} \frac{3}{2} n_p (i_{s,\text{cut-in}}^{k,\text{MTPV}}(\omega_k))^\top \times \mathbf{J} (\mathbf{L}_s^k i_{s,\text{cut-in}}^{k,\text{MTPV}}(\omega_k) + \psi_{\text{pm}}^k). \quad (43)$$

Note that maximally feasible FW torque and MTPV cut-in torque are equivalent at the MTPV cut-in angular velocity, i.e.

$$m_{m,\text{feas}}^{\text{FW}}(\omega_{k,\text{cut-in}}^{\text{MTPV}}) = m_{m,\text{cut-in}}^{\text{MTPV}}(\omega_{k,\text{cut-in}}^{\text{MTPV}}),$$

since also the respective current vectors do equal, i.e. $i_{s,\text{feas}}^{k,\text{FW}}(\omega_{k,\text{cut-in}}^{\text{MTPV}}) = i_{s,\text{cut-in}}^{k,\text{MTPV}}(\omega_{k,\text{cut-in}}^{\text{MTPV}})$ (see green square ■ and orange square ■ in Figure 5(c)). Please also note that green square ■ and orange square ■ are actually located at the same intersection point in the current locus; for illustration, both squares are slightly shifted away from their original location to make both squares visible.

5.2 Selection of the optimal operation strategy

The operation management is illustrated in Figure 5(a). It is divided into two parts: the offline and the online computation. The inputs to the online and offline parts are the machine parameters $L_s^d, L_s^q, L_m, \psi_{pm}^k, R_s, n_p, \hat{i}_{max}$ and \hat{u}_{max} , and the constant operation management parameters nominal torque $m_{m,nom} = m_{m,nom}^{MC}(\hat{i}_{max})$ and the MTPV cut-in speed $\omega_{k,cut-in}^{MTPV}$ (both can be computed offline).

Once the operation management is initialised, the feedforward torque controller is ready for online computation and, at each sampling instant $t = kT_s$ (with index $k \in \mathbb{N}$ and cycle period T_s), the actual values of the electrical speed $\omega_k(t)$ (measured or estimated) and reference torque $m_{m,ref}(t)$ (coming from an outer control loop) serve as inputs to the online part. First, if necessary, the reference torque is saturated, i.e.

$$\begin{aligned} \bar{m}_{m,ref} &:= \text{sat}_{m_{m,nom}}(m_{m,ref}) \\ &:= \begin{cases} \text{sign}(m_{m,ref})m_{m,nom}, & |m_{m,ref}| > m_{m,nom} \\ m_{m,ref}, & |m_{m,ref}| \leq m_{m,nom}, \end{cases} \end{aligned} \quad (44)$$

to guarantee that $\bar{m}_{m,ref} \in [-m_{m,nom}, m_{m,nom}]$ remains within the nominal (hence admissible) torque range. The remaining three operation management parameters, such as (i) feasible MTPC speed $\omega_{k,feas}^{MTPC}(\bar{m}_{m,ref})$ (a function of the saturated torque reference; see (41) and blue dashed line (.....) in Figure 5(b)), (ii) feasible FW torque $m_{m,feas}^{FW}(\omega_k)$ (a function of actual speed, see (42)), and (iii) the MTPV cut-in torque $m_{m,cut-in}^{MTPV}(\omega_k)$ (a function of actual speed, see (43)) must *exclusively* be computed, if the decision tree reaches the respective decision points (diamonds) in Figure 5(a). This exclusive (only if needed) computation reduces – besides the proposed analytical solutions – the computational burden of the real-time implementation. The selection of the optimal strategy is based on the decision tree (flow chart) depicted in Figure 5(a) and is explained in the following:

- **MTPC:** If $|\omega_k| \leq \omega_{k,feas}^{MTPC}(\bar{m}_{m,ref})$, i.e. ‘Yes’ in Figure 5(a), the optimal current reference vector $i_{s,ref}^k = i_{s,ref}^{k,MTPC}$ is determined by the intersection point of torque hyperbola and MTPC hyperbola, i.e. $i_{s,ref}^k \in \mathbb{T}(\bar{m}_{m,ref}) \cap \text{MTPC}$ (see Table 1). For this case, the feasible torque is solely limited by the nominal torque $m_{m,nom}$. In Figure 5(c) (torque over speed) and Figure 5(c) (current locus), the corresponding MTPC operation mode is marked by the blue shaded area and the thick blue line (—).
- **MC:** If $\omega_{k,feas}^{MTPC}(\bar{m}_{m,ref}) < |\omega_k| \leq \omega_{k,cut-in}^{MTPV}$ and $|\bar{m}_{m,ref}| > m_{m,feas}^{FW}(\omega_k)$, i.e. ‘No/Yes/No’ in Figure 5(a), the optimal current reference

vector $i_{s,ref}^k = i_{s,ref}^{k,MC}$ is given by the intersection $\partial\mathbb{I}(\hat{i}_{max}) \cap \partial\mathbb{V}(\omega_k, \hat{u}_{max})$ of current circle and voltage ellipse (see Table 1). Note that feasible MTPC speed $\omega_{k,feas}^{MTPC}(m_{m,ref})$ and feasible FW torque $m_{m,feas}^{FW}(\omega_k)$ decrease for increasing values of (saturated) reference torque $\bar{m}_{m,ref}$ and angular velocity ω_k , respectively (see Figure 5(b)). The MC operation mode is marked by the thick orange line (—) in Figure 5(b,c), respectively.

- **FW:** If $\omega_{k,feas}^{MTPC}(\bar{m}_{m,ref}) < |\omega_k| \leq \omega_{k,cut-in}^{MTPV}$ and $|\bar{m}_{m,ref}| \leq m_{m,feas}^{FW}(\omega_k)$ or $|\omega_k| > \omega_{k,cut-in}^{MTPV}$ and $|\bar{m}_{m,ref}| < m_{m,cut-in}^{MTPV}(\omega_k)$, i.e. ‘No/Yes/Yes’ or ‘No/No/Yes’ in Figure 5(a), the machine is operated in FW mode. The optimal reference current vector $i_{s,ref}^k = i_{s,ref}^{k,FW}$ is obtained by the intersection $\mathbb{T}(\bar{m}_{m,ref}) \cap \partial\mathbb{V}(\omega_k, \hat{u}_{max})$ of torque hyperbola and voltage ellipse (see Table 1 and dotted green line (.....) in Figure 5(b,c)). Note that the MTPV cut-in torque $m_{m,cut-in}^{MTPV}(\omega_k)$ decreases for increasing speed ω_k (since the voltage ellipse shrinks). The operation in FW is highlighted by the light green shaded area in Figure 5(b,c), respectively.
- **MTPV:** If $|\omega_k| > \omega_{k,cut-in}^{MTPV}$ and $|\bar{m}_{m,ref}| \geq m_{m,cut-in}^{MTPV}(\omega_k)$, i.e. ‘No/No/No’ in Figure 5(a), MTPV becomes active and the optimal reference current vector $i_{s,ref}^k = i_{s,ref}^{k,MTPV}$ is computed by finding the intersection $\partial\mathbb{V}(\omega_k, \hat{u}_{max}) \cap \text{MTPV}$ of voltage ellipse and MTPV hyperbola (see Table 1). MTPV operation is indicated by the thick light blue line (—) in Figure 5(b,c), respectively.

In view of Remark 4.6, the operation strategy MTPF is not considered. It only gives a rough approximation of the MTPV strategy, and the MTPV strategy should be preferred for implementation, since it is more accurate and yields a higher efficiency.

6. Implementation

The theoretical derivations are backed by the following two implementations and their comparison with the numerical approaches: computer simulation of the algorithm to find the roots of a fourth-order polynomial analytically (see Appendix A.1.3), and the real-time implementation of the proposed analytical MTPC strategy and its application to a *nonlinear* RSM in the laboratory.

6.1 Performance comparison of numerical and proposed analytical solver to find the roots of fourth-order polynomials

Solving fourth-order polynomials analytically is the primary task in the presented approach. It has been

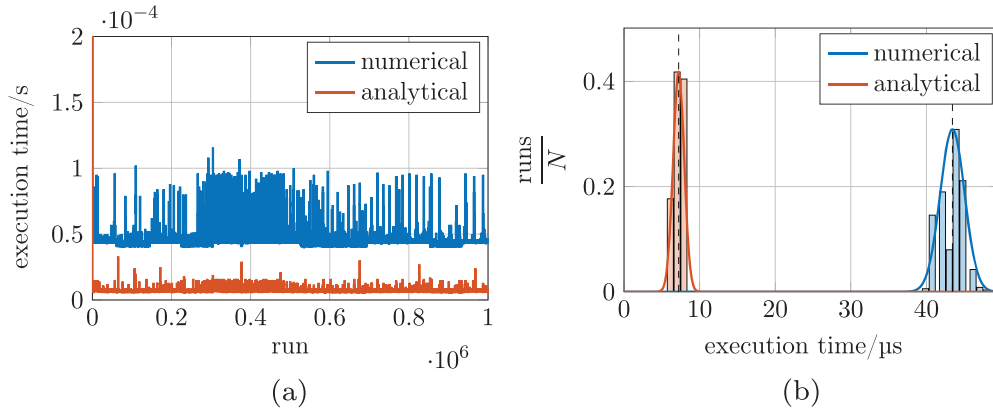


Figure 6. Results of the performance comparison of numerical and analytical solution to find the roots of fourth-order polynomials: (a) execution times for $N = 10^6$ and (b) histograms of the test data (in ascending order) with average execution times $\mu_n = 43.4 \cdot 10^{-6}$ s and $\mu_a = 7.23 \cdot 10^{-6}$ s, and standard deviations $\sigma_n = 1.61 \cdot 10^{-6}$ s and $\sigma_a = 0.73 \cdot 10^{-6}$ s for numerical and analytical solution, respectively.

implemented in MATLAB R2016b as MEX code (C function) and compared with the built-in *roots* function (C function based on *eig*) using a numerical approach. The comparison has been conducted by measuring the execution times of the respective algorithms for input polynomials with randomly generated coefficients. The five coefficients $c_i = b_i^{e_i}$ of the fourth-order polynomial in (A10) were generated by random bases $b_i \in [0, 1]$ (double precision) and random integer exponents $e_i \in [-10, 10]$ for $i \in \{0, 1, \dots, 4\}$. Moreover, the test has been repeated for $N = 10^6$ runs in order to mitigate unpredictable delay times due to task scheduling or memory issues on the test PC. The results of the experiment are depicted in Figure 6. A comparison of the histograms allows to draw two main conclusions: (i) on average, the analytical solution is about six times faster, and (ii) the standard deviation of the numerical approach is remarkably higher which makes the estimation of the execution time more difficult

for the numerical approach. Moreover, it is important to note that, in view of the decision tree in Figure 5(a), the roots of fourth-order polynomials must be computed several times; e.g. for MTPV, the roots of *three* fourth-order polynomials must be found: twice for the computation of the online operation management parameters $\omega_{k,feas}^{MTPC}(\bar{m}_{m,ref})$ and $m_{m,cut-in}^{MTPV}(\omega_k)$, and once for the computation of the optimal reference current vector (see Figure 5(a) and recall Section 5.1). In this case, the computation of the analytical solution is (at least) 18 times faster than that of the numerical solution.

6.2 Measurement results

The analytical computation of the MTPC reference current vector $\mathbf{i}_{s,ref}^k = \mathbf{i}_{s,ref}^{k,MTPC}$ (see Table 1) was implemented at a laboratory set-up and measurements were conducted in order to verify the presented theory. Instead of employing a fairly linear PMSM, a highly nonlinear RSM

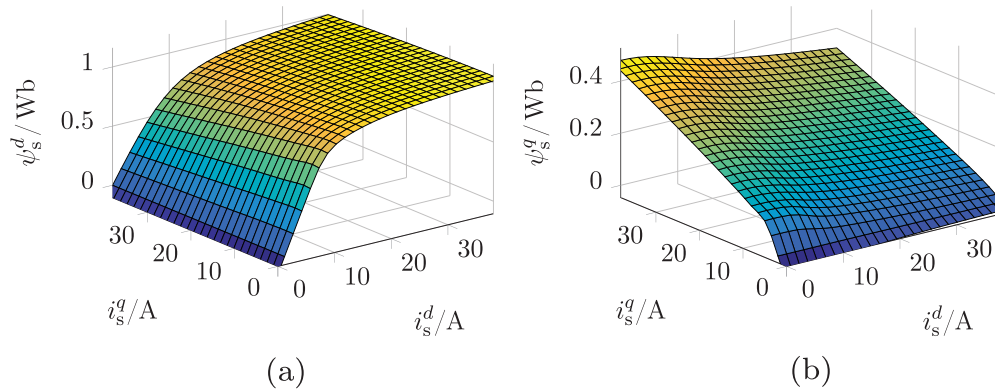


Figure 7. Nonlinear flux linkages (a) $\psi_s^d(i_s^d, i_s^q)$ and (b) $\psi_s^q(i_s^d, i_s^q)$ of a custom-built 9.6 kW RSM with parameters as in (45) (the maps are only shown for the first quadrant, i.e. $i_s^d \geq 0$ and $i_s^q \geq 0$, where a positive machine torque can be produced).

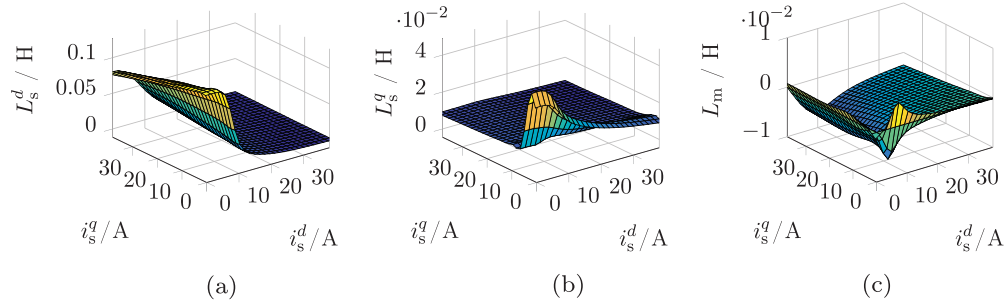


Figure 8. Nonlinear components (a) $L_s^d(i_s^d, i_s^q)$, (b) $L_s^q(i_s^d, i_s^q)$ and (c) $L_m(i_s^d, i_s^q)$ of the inductance matrix (46) (the inductances are only shown for the first quadrant, i.e. $i_s^d \geq 0$ and $i_s^q \geq 0$).

served as device under test so as to prove the robustness of the presented theory and its industrial applicability. Finally, the measurement results of the analytical MTPC approach were compared with the numerically calculated reference currents.

6.2.1 Measurement set-up and scenario

The presented theory has been implemented and verified experimentally on a custom-build 9.6 KW RSM (courtesy of Prof. Maarten Kamper, Stellenbosch University, South Africa) with the parameters

$$\left. \begin{aligned} R_s &= 0.4 \Omega, \quad \omega_{k, \text{nom}} = \frac{2\pi}{60\text{s}} \cdot 1500 \text{ rpm} = 157.07 \frac{\text{rad}}{\text{s}}, \\ m_{m, \text{nom}} &= 61 \text{ N m}, \\ \hat{i}_{\text{max}} &= 29.7 \text{ A}, \quad \text{and} \quad \hat{u}_{\text{max}} = 590 \text{ V}, \end{aligned} \right\} \quad (45)$$

and the nonlinear flux linkage maps as depicted in Figure 7 (maps were obtained from FEM). The current-dependent inductances, shown in Figure 8, were calculated by numerical differentiation of the flux maps with respect to the currents. The overall laboratory set-up is depicted in Figure 9 and comprises the dSPACE real-time system (A) with processor board DS1007 and various extensions and I/O boards, two 22 k W SEW inverters (B1, B2) in back-to-back configuration sharing a common DC link, the HOST-PC (C) running MATLAB/Simulink with RCPHIL R2015b and dSPACE ControlDesk 5.5 for rapid-prototyping, data acquisition and evaluation, the custom-built 9.6 kW RSM (D1) as device under test and a 14.5 kW SEW PMSM (D2) to regulate the mechanical speed. Moreover, the Lorenz[®] torque sensor (E) allows to measure the mechanical output power

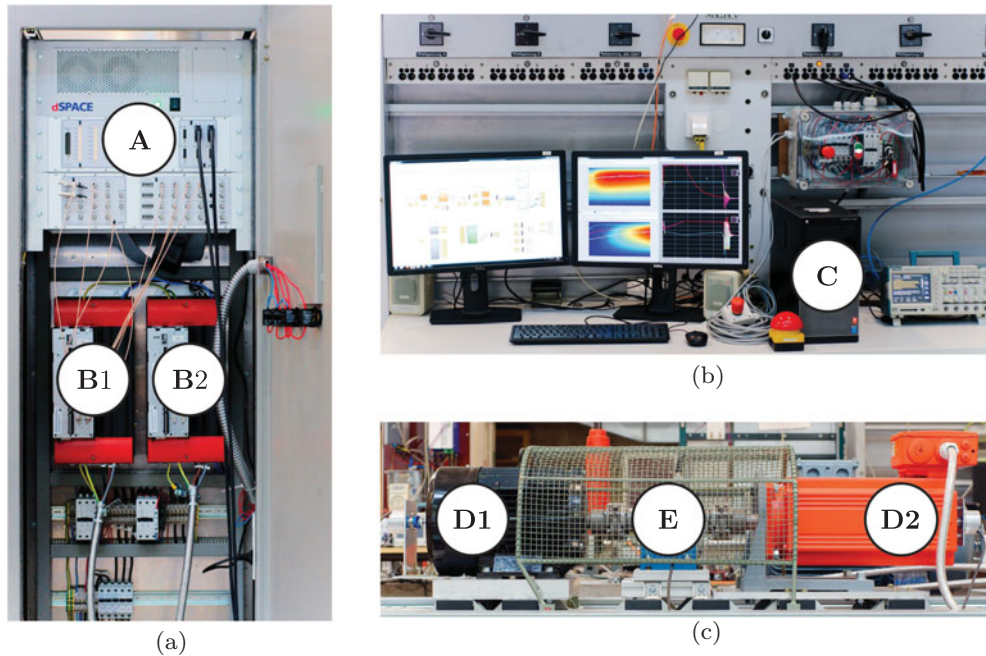


Figure 9. Laboratory set-up with (a) dSPACE real-time system (A), voltage-source inverters (B1) and (B2) connected back-to-back, (b) Host-PC (C) for rapid-prototyping, and (c) RSM (D1) and PMSM (D2), and torque sensor (E).

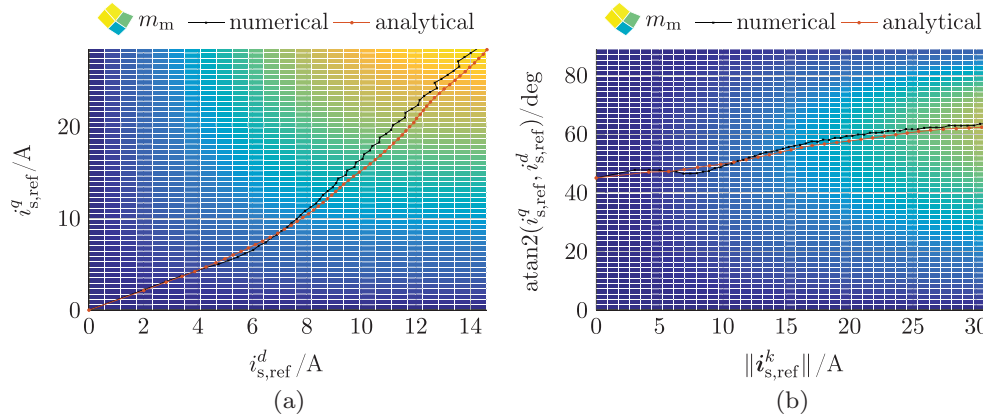


Figure 10. Measurement results for a nonlinear custom-build 9.6 kW RSM at $150 \frac{\text{rad}}{\text{s}}$: Comparison of the optimal reference currents $\mathbf{i}_{s,\text{ref}}^k = (i_{s,\text{ref}}^d, i_{s,\text{ref}}^q)^\top$ for MTPC mode (a) in Cartesian coordinates and (b) in polar coordinates computed by the conventional numerical and the proposed analytical solution (for the experiment, the reference torque $m_{m,\text{ref}}$ was stepped up from zero to nominal torque by increments of 1 N m and held constant for two seconds).

(not used in here). The experiments were conducted for MTPC operation at the constant speed $\omega_k \approx \omega_{k,\text{nom}}$ and for a positive reference torque only (operation as motor). The reference torque $m_{m,\text{ref}}$ was increased stepwise by increments of 1 Nm from zero to nominal torque $m_{m,\text{nom}}$ and held constant at each step for two seconds. The nonlinear flux linkages and inductances were tracked online and fed into the feedforward torque controller at each sampling step to improve the accuracy of the presented analytic MTPC algorithm.

To be able to express the nonlinear RSM dynamics in the form (1) with affine flux linkage (2), the nonlinear flux linkage (as depicted in Figure 7) of the RSM were linearised online (at each sampling instant) by invoking the following first-order Taylor expansion

$$\begin{aligned} \boldsymbol{\psi}_s^k(\mathbf{i}_s^k) &\approx \underbrace{\frac{d\boldsymbol{\psi}_s^k(\mathbf{i}_s^k)}{d\mathbf{i}_s^k}}_{=: \mathbf{L}_s^k = \mathbf{L}_s^k(\mathbf{i}_{s,0}^k)} \bigg|_{\mathbf{i}_s^k = \mathbf{i}_{s,0}^k} (\mathbf{i}_s^k - \mathbf{i}_{s,0}^k) + \boldsymbol{\psi}_s^k(\mathbf{i}_{s,0}^k) \\ &= \mathbf{L}_s^k \mathbf{i}_s^k + \underbrace{\boldsymbol{\psi}_s^k(\mathbf{i}_{s,0}^k) - \mathbf{L}_s^k \mathbf{i}_{s,0}^k}_{=: \boldsymbol{\psi}_m^k = \boldsymbol{\psi}_m^k(\mathbf{i}_{s,0}^k)} \end{aligned} \quad (46)$$

around the actual operation point $\mathbf{i}_{s,0}^k := (i_{s,0}^d, i_{s,0}^q)^\top \in \mathbb{R}^2$ (actual current vector). The linearised (locally affine) flux linkage in (46) with the differential inductance matrix $\mathbf{L}_s^k(\mathbf{i}_{s,0}^k) := [L_s^d(\mathbf{i}_{s,0}^k), L_m(\mathbf{i}_{s,0}^k); L_m(\mathbf{i}_{s,0}^k), L_s^q(\mathbf{i}_{s,0}^k)] \in \mathbb{R}^{2 \times 2}$ and the ‘magnetisation’ flux linkage vector $\boldsymbol{\psi}_m^k := (\psi_m^d, \psi_m^q)^\top$ is clearly similar to the affine flux linkage in (2) (set $\boldsymbol{\psi}_{\text{pm}}^k = \boldsymbol{\psi}_m^k$). Finally, the analytical solution to compute the optimal MTPC reference current vector $\mathbf{i}_{s,\text{ref}}^k = \mathbf{i}_{s,\text{ref}}^{k,\text{MTPC}}$ was implemented. The obtained reference

currents for numerical and analytical solution were low-pass filtered (with time constant $T_f = 50T_s$) and their mean values over the 2 s-time interval (where the torque reference was held constant) were computed for each torque reference step.

6.2.2 Discussion of the results

The computed reference currents of both, the numerical and the analytical torque feedforward controller, are depicted in Figure 10. Results in the Cartesian coordinates are shown in Figure 10(a), where in Figure 10(b), polar coordinates were used. The former shows, in particular for currents with small magnitude, that numerical and analytical results coincide with high accuracy. Only for larger currents (beyond $i_s^d \geq 8$ A), a deviation can be observed. However, it remains within an acceptable range which becomes clear if the polar coordinate representation is taken into account. Here, the numerical solution shows an unexpected shape in the lower current magnitude region which could be an error due to a deteriorated interpolation and/or a deteriorated accuracy of the numerical solver. Nonetheless, the angle difference is small over the whole operation range and the results show that both approaches give almost identical reference currents.

7. Conclusion and future work

This work introduced a unified theory to solve the optimal feedforward torque control problem of anisotropic SMs *analytically* while stator resistance and cross-coupling (mutual) inductance are explicitly considered. For all operation strategies such as (a) MTPC (which, in literature, is often called MTPA), (b) MC, (c) FW and

(d) MPTV or MTPF, analytical expressions for the optimal reference currents are derived. To the best knowledge of the authors, such analytical solutions *including* stator resistance and mutual inductance for MTPC, MC, FW, MTPV and MTPF of anisotropic SMs were scarcely investigated this far or not available at all.

The obtained analytical solutions are attractive, since they are easier to implement, more accurate and faster to compute. Moreover, for the operation management of the machine, algorithms were proposed which allow to compute the crucial operation management parameters based on which the actually optimal operation strategy can easily be selected online. The theoretical findings were illustrated by (i) a performance comparison of the conventional numerical and the proposed analytical algorithm for finding the roots of a fourth-order polynomial and (ii) measurement results at a nonlinear reluctance synchronous machine (for MTPC). The implemented analytical solution is obtained significantly faster and matches with the conventional numerical solution with high accuracy.

Future work will focus on the extension of the unified theory to nonlinear flux linkages (without the need of linearisation) and the consideration of iron losses in the optimisation problem as well.

Notes

1. The terminology ‘Maximum Torque per Current (MPTC)’ will be used in this paper (see also Remark 4.2).
2. That is, the synchronously rotating $k = (d, q)$ -coordinate system with orthogonal axes d and q after Clarke and Park transformation (Dirscherl et al., 2015; Teodorescu et al., 2011).
3. The factor $3/2$ is due to an amplitude-correct Clarke transformation (Schröder, 2009, Section 16.7).
4. Note that the mutual inductance L_m changes its sign with the negative product of the currents, i.e. $\text{sign}(L_m) = -\text{sign}(i_s^d \cdot i_s^q)$ (Hackl et al., 2015, Figure 2).
5. Note that, for some vectors $\mathbf{x}, \mathbf{c} \in \mathbb{R}^n$ and a symmetric matrix $\mathbf{M} = \mathbf{M}^\top \in \mathbb{R}^{n \times n}$, the following hold: $(\frac{d\mathbf{c}^\top \mathbf{x}}{dx})^\top = (\frac{dc_1^\top}{dx_1}, \dots, \frac{dc_n^\top}{dx_n})^\top = (c_1, \dots, c_n)^\top = \mathbf{c}$ and $(\frac{d\mathbf{x}^\top \mathbf{M} \mathbf{x}}{dx})^\top = (\frac{dx_1^\top \mathbf{M} \mathbf{x}}{dx_1}, \dots, \frac{dx_n^\top \mathbf{M} \mathbf{x}}{dx_n})^\top = (\mathbf{M} + \mathbf{M}^\top) \mathbf{x} = 2\mathbf{M} \mathbf{x}$ (see Bernstein, 2009, Proposition 10.7.1 i)).
6. The i th leading principle minor of a matrix is the determinant of the (i, i) -north-western sub-matrix of the matrix (Bernstein, 2009, Proposition 8.2.7).
7. That is, for all $\gamma \in \mathbb{R}$ and $\mathbf{A} \in \mathbb{R}^{n \times n}$, the following holds $\det(\gamma \mathbf{A}) = (\gamma)^n \det(\mathbf{A})$. Hence, the application of the Sylvester’s criterion to negative definite matrices yields alternating signs of the leading principle minors.
8. For case (iii), substitute \mathbf{y} for \mathbf{x} .

Disclosure statement

No potential conflict of interest was reported by the authors.

Funding

This project has received funding from the European Union’s Horizon 2020 research and innovation programme under the Marie Skłodowska-Curie [grant number 642682]; and from the Bavarian Ministry for Education, Culture, Science and Art.

References

- Abramowitz, M., Stegun, I., & Miller, D. (1964). *Handbook of mathematical functions with formulas, graphs and mathematical tables*. (10th ed.). Vol. (Dec. 1972) of *Applied Mathematics Series*. Washington, DC: National Bureau of Standards.
- Ahn, J., Lim, S. B., Kim, K. C., Lee, J., Choi, J. H., Kim, S., & Hong, J. P. (2007). Field weakening control of synchronous reluctance motor for electric power steering. *IET Electric Power Applications*, 1, 565–570.
- Bedetti, N., Calligaro, S., & Petrella, R. (2016). Stand-still self-identification of flux characteristics for synchronous reluctance machines using novel saturation approximating function and multiple linear regression. *IEEE Transactions on Industry Applications*, 52, 3083–3092.
- Bernstein, D. S. (2009). *Matrix mathematics – Theory, facts, and formulas with application to linear system theory*. (2nd ed.). Princeton, NJ: Princeton University Press.
- Boldea, I., Tutelea, L. N., Parsa, L., & Dorrell, D. (2014). Automotive electric propulsion systems with reduced or no permanent magnets: An overview. *IEEE Transactions on Industrial Electronics*, 61, 5696–5711.
- Boyd, S., & Vandenberghe, L. (2004). *Convex optimization*. (7th printing with corrections 2009). Cambridge: Cambridge University Press.
- Colby, R. S., & Novotny, D. W. (1988). An efficiency-optimizing permanent-magnet synchronous motor drive. *IEEE Transactions on Industry Applications*, 24, 462–469.
- Calleja, C., de Heredia, A. L., Gaztanaga, H., Nieva, T., & Aldasoro, L. (2016). Validation of a modified direct-self-control strategy for PMSM in railway-traction applications. *IEEE Transactions on Industrial Electronics*, 63, 5143–5155.
- Cavallaro, C., Di Tommaso, A., Miceli, R., Raciti, A., Galluzzo, G., & Trapanese, M. (2005). Efficiency enhancement of permanent-magnet synchronous motor drives by online loss minimization approaches. *IEEE Transactions on Industrial Electronics*, 52, 1153–1160.
- Cheng, B., & Tesch, T. R. (2010). Torque feedforward control technique for permanent-magnet synchronous motors. *IEEE Transactions on Industrial Electronics*, 57, 969–974.
- de Almeida, A., Ferreira, F., & Fong, J. (2011). Standards for efficiency of electric motors. *Industry Application Magazine*, 17, 12–19.
- Dirscherl, C., Hackl, C., & Schechner, K. (2015). Modellierung und Regelung von modernen Windkraftanlagen: Eine Einführung [Modeling and control of modern wind turbine systems: An introduction]. In D. Schröder (Ed.), *Elektrische Antriebe – Regelung von Antriebssystemen [Electrical drives – Control of electrical drive systems]* (Chapter 24, pp. 1540–1614). Berlin Heidelberg: Springer-Verlag.
- Eldeeb, H., Hackl, C. M., & Kullick, J. (2016). Efficient operation of anisotropic synchronous machines for wind energy

- systems. *Journal of Physics: Conference Series*, 753, 112009. doi: 10.1088/1742-6596/753/11/112009
- Finken, T. (2012). *Fahrzyklusgerechte Auslegung von permanent-erregten Synchronmaschinen für Hybrid- und Elektrofahrzeuge [Dimensioning of permanent-magnet synchronous machines for hybrid and electric vehicles based on driving cycles]* (PhD thesis). Aachen: Insitut für elektrische Maschinen, RWTH.
- Foo, G., & Zhang, X. N. (2016). Robust direct torque control of synchronous reluctance motor drives in the field weakening region. *IEEE Transactions on Power Electronics*, 99, 1–1.
- Gemassmer, T. (2015). *Effiziente und dynamische Drehmomenteinprägung in hoch ausgenutzten Synchronmaschinen mit eingebetteten Magneten [Efficient and dynamic torque generation in optimized synchronous machines with buried magnets]* (PhD thesis). Karlsruhe: Elektrotechnisches Institut, KIT.
- Hackl, C. M. (2015). Current PI-funnel control with anti-windup for synchronous machines. In *Proceedings of the 54th IEEE Conference on Decision and Control (CDC)* (pp. 1997–2004). Osaka: IEEE.
- Hackl, C. M., Kamper, M. J., Kullick, J. & Mitchell, J. (2015). Nonlinear PI current control of reluctance synchronous machines. Retrieved from <https://arxiv.org/pdf/1512.09301>.
- Hackl, C. M., Kamper, M. J., Kullick, J., & Mitchell, J. (2016). Current control of reluctance synchronous machines with online adjustment of the controller parameters. In *Proceedings of the 2016 IEEE International Symposium on Industrial Electronics (ISIE 2016)* (pp. 153–160). Santa Clara, CA: IEEE.
- Horlbeck, L., & Hackl, C. (2016). Analytical solution for the MTPV hyperbola including the stator resistance. In *Proceedings of the IEEE International Conference on Industrial Technology (ICIT 2016)* (pp. 1060–1067). Taipei: IEEE.
- Huber, T., Peters, W., & Böcker, J. (2015). Voltage controller for flux weakening operation of interior permanent magnet synchronous motor in automotive traction applications. In *Proceedings of the IEEE International Electric Machines and Drives Conference* (pp. 1078–1083). IEEE.
- Jung, S. Y., Hong, J., & Nam, K. (2013). Current minimizing torque control of the IPMSM using Ferrari's method. *IEEE Transactions on Power Electronics*, 28, 5603–5617.
- Kim, J., Jeong, I., Nam, K., Yang, J., & Hwang, T. (2015). Sensorless control of PMSM in a high-speed region considering iron loss. *IEEE Transactions on Industrial Electronics*, 62, 6151–6159.
- Lemmens, J., Vanassche, P., & Driesen, J. (2015). PMSM drive current and voltage limiting as a constraint optimal control problem. *IEEE Journal of Emerging and Selected Topics in Power Electronics*, 3, 326–338.
- Mademlis, C., Kioskeridis, I., & Margaris, N. (2004). Optimal efficiency control strategy for interior permanent-magnet synchronous motor drives. *IEEE Transactions on Energy Conversion*, 19, 715–723.
- Morimoto, S., Takeda, Y., Hirasa, T., & Taniguchi, K. (1990). Expansion of operating limits for permanent magnet motor by current vector control considering inverter capacity. *IEEE Transactions on Industry Applications*, 26, 866–871.
- Ni, R., Xu, D., Wang, G., Ding, L., Zhang, G., & Qu, L. (2015). Maximum efficiency per ampere control of permanent-magnet synchronous machines. *IEEE Transactions on Industry Applications*, 62, 2135–2143.
- Niazi, P., Toliyat, H. A., & Goodarzi, A. (2007). Robust maximum torque per ampere (MTPA) control of PM-assisted SynRM for traction applications. *IEEE Transactions on Vehicular Technology*, 56, 1538–1545.
- Nickalls, R. (2009). The quartic equation: Invariants and Euler's solution revealed. *Mathematical Gazette*, 93(526), 66–75.
- Nakamura, Y., Kudo, T., Ishibashi, F., & Hibino, S. (1995). High-efficiency drive due to power factor control of a permanent magnet synchronous motor. *IEEE Transactions on Power Electronics*, 10, 247–253.
- Panaiteescu, R. C., & Topa, I. (1998). Optimal control method for PMSM by minimization of electrical losses. *Proceedings of IEEE International Conference on Optimization of Electrical and Electronic Equipments (OPTIM)*, 2, 451–456.
- Peters, W., Wallscheid, O., & Böcker, J. (2015). Optimum efficiency control of interior permanent magnet synchronous motors in drive trains of electric and hybrid vehicles. In *Proceedings of the 17th European Conference on Power Electronics and Applications (EPE'15 ECCE-Europe)* (pp. 1–10). IEEE.
- Preindl, M., & Bolognani, S. (2013a). Model predictive direct torque control with finite control set for PMSM drive systems. Part 1: Maximum torque per ampere operation. *IEEE Transactions on Industrial Informatics*, 9, 1912–1921.
- Preindl, M., & Bolognani, S. (2013b). Model predictive direct torque control with finite control set for PMSM drive systems. Part 2: Field weakening operation. *IEEE Transactions on Industrial Informatics*, 9, 648–657.
- Preindl, M., & Bolognani, S. (2015). Optimal state reference computation with constrained MTPA criterion for PM motor drives. *IEEE Transactions on Power Electronics*, 30, 4524–4535.
- Rees, E. (1922). Graphical discussion of the roots of a quartic equation. *The American Mathematical Monthly*, 29(2), 51–55.
- Schmidt, E. (2014). Synchronous reluctance machines with high-anisotropy rotors – comparison of their operational characteristics. In *Proceedings of the Australasian Universities Power Engineering Conference* (pp. 1–6). IEEE.
- Schröder, D. (2009). *Elektrische Antriebe – Regelung von Antriebssystemen [Electrical drives - Control of electrical drive systems]*. Berlin Heidelberg : Springer-Verlag.
- Schoonhoven, G., & Uddin, M. N. (2016). MTPA- and FW-based robust nonlinear speed control of IPMSM drive using Lyapunov stability criterion. *IEEE Transactions on Industry Applications*, 52, 4365–4374.
- Tang, Z., Li, X., Dusmez, S., & Akin, B. (2016). A new V/f-based sensorless MTPA control for IPMSM Drives. *IEEE Transactions on Power Electronics*, 31, 4400–4415.
- Teodorescu, R., Liserre, M., & Rodríguez, P. (2011). *Grid converters for photovoltaic and wind power systems*. Chichester: John Wiley & Sons.
- Tursini, M., Chiricozzi, E. & Petrella, R. (2010). Feedforward flux-weakening control of surface-mounted permanent-magnet synchronous motors accounting for resistive voltage drop. *IEEE Transactions on Industrial Electronics*, 57, 440–448.
- Ueda, K., Morimoto, S., Inoue, Y., & Sanada, M. (2014, May). A novel control method in flux-weakening region for efficient operation of interior permanent magnet synchronous motor. In *Proceedings IEEE International Power Electronics Conference (IPEC-ECCE ASIA)* (pp. 312–317). IEEE.

Urasaki, N., Senjyu, T., & Uezato, K. (2003). A novel calculation method for iron loss resistance suitable in modeling permanent-magnet synchronous motors. *IEEE Transactions on Energy Conversion*, 18, 41–47.

Vaez, S., John, V. I., & Rahman, M. A. (1997, June). Adaptive loss minimization control of inverter-fed IPM motor drives. In *Proceedings IEEE Power Electronics Specialists Conference (PESC)* (Vol. 2, pp. 861–868). IEEE.

Wang, Y., Ionel, D. M., Jiang, M., & Stretz, S. J. (2016). Establishing the relative merits of synchronous reluctance and PM-assisted technology through systematic design optimization. *IEEE Transactions on Industry Applications*, 52, 2971–2978.

Zhang, P., Ionel, D., & Demerdash, N. (2016). Saliency ratio and power factor of IPM motors with distributed windings optimally designed for high efficiency and low cost applications. *IEEE Transactions on Industry Applications*, 99, 1–1.

Zippel, R. (2012). *Effective polynomial computation. The Springer International Series in Engineering and Computer Science*. Boston: Kluwer Academic Publishers/Springer US.

Appendices

Appendix 1. Quadrics

In this appendix, all necessary mathematical derivations are presented for two general quadrics given by

$$\begin{aligned} Q_A(\mathbf{x}) &:= \mathbf{x}^\top \mathbf{A} \mathbf{x} + 2\mathbf{a}^\top \mathbf{x} + \alpha & \text{and} \\ Q_B(\mathbf{x}) &:= \mathbf{x}^\top \mathbf{B} \mathbf{x} + 2\mathbf{b}^\top \mathbf{x} + \beta, \end{aligned} \quad (\text{A1})$$

where

$$\left. \begin{aligned} \mathbf{A} = \mathbf{A}^\top &:= \begin{bmatrix} a_{11} & a_{12} \\ a_{12} & a_{22} \end{bmatrix} \in \mathbb{R}^{2 \times 2}, \\ \mathbf{a} &:= \begin{pmatrix} a_1 \\ a_2 \end{pmatrix} \in \mathbb{R}^2, \alpha \in \mathbb{R}, \\ \mathbf{B} = \mathbf{B}^\top &:= \begin{bmatrix} b_{11} & b_{12} \\ b_{12} & b_{22} \end{bmatrix} \in \mathbb{R}^{2 \times 2}, \\ \mathbf{b} &:= \begin{pmatrix} b_1 \\ b_2 \end{pmatrix} \in \mathbb{R}^2 \text{ and } \beta \in \mathbb{R}. \end{aligned} \right\} \quad (\text{A2})$$

The main goal is to explain in detail how analytical solutions to the MTPC, MTPV and MTPF optimisation problems can be obtained and how analytical solutions for the intersection points of two general quadrics can be found. As it will be shown, all problems can be solved by finding the roots of a fourth-order *quartic polynomial* for which (luckily) still an analytical solutions exists.

A.1. Formulation of the optimisation problem with equality constraints

The optimisation problems MTPC, MTPV and MTPF can be formulated in a general framework as optimisation problems with equality constraint by invoking the

quadrics $Q_A(\mathbf{i}_s^k)$ and $Q_B(\mathbf{i}_s^k)$ in (A1) as follows:

$$\begin{aligned} \mathbf{i}_{s,\text{ref}}^k &:= \arg \max_{\mathbf{i}_s^k} - \underbrace{\left((\mathbf{i}_s^k)^\top \mathbf{A} \mathbf{i}_s^k + 2\mathbf{a}^\top \mathbf{i}_s^k + \alpha \right)}_{=: Q_A(\mathbf{i}_s^k)} \\ \text{s.t. } &\underbrace{(\mathbf{i}_s^k)^\top \mathbf{B} \mathbf{i}_s^k + 2\mathbf{b}^\top \mathbf{i}_s^k + \beta}_{=: Q_B(\mathbf{i}_s^k)} = 0. \end{aligned} \quad (\text{A3})$$

The first idea, based on quadrics, was presented in Eldeeb et al. (2016) for the MTPC strategy. The optimisation problem (A3) can be reformulated as *Lagrangian* (see Boyd & Vandenberghe 2004, Chapter 5), i.e.

$$\begin{aligned} \mathcal{L}(\mathbf{i}_s^k, \lambda) &:= -Q_A(\mathbf{i}_s^k) + \lambda Q_B(\mathbf{i}_s^k) \\ &\stackrel{(\text{A3})}{=} -\left[(\mathbf{i}_s^k)^\top \mathbf{A} \mathbf{i}_s^k + 2\mathbf{a}^\top \mathbf{i}_s^k + \alpha \right] \\ &\quad + \lambda \left[(\mathbf{i}_s^k)^\top \mathbf{B} \mathbf{i}_s^k + 2\mathbf{b}^\top \mathbf{i}_s^k + \beta \right], \end{aligned} \quad (\text{A4})$$

where the (possibly complex) Lagrangian multiplier $\lambda \in \mathbb{C}$ must be introduced for the equality constraint. For the three different optimisation problems MTPC, MTPF and MTPV, the matrices \mathbf{A} , \mathbf{B} , vectors \mathbf{a} , \mathbf{b} and scalars α , β must be chosen accordingly as specified in the following:

- MTPC: $\mathbf{A} = \mathbf{I}_2$, $\mathbf{a} = (0, 0)^\top$, $\alpha = 0$ and $\mathbf{B} = \mathbf{T}$, $\mathbf{b} = \mathbf{t}$ and $\beta = \tau(m_{m,\text{ref}})$,
- MTPV: $\mathbf{A} = \mathbf{V}(\omega_k)$, $\mathbf{a} = \mathbf{v}(\omega_k)$, $\alpha = \nu(\omega_k, \hat{u}_{\text{max}})$ and $\mathbf{B} = \mathbf{T}$, $\mathbf{b} = \mathbf{t}$ and $\beta = \tau(m_{m,\text{ref}})$, and
- MTPF: $\mathbf{A} = \mathbf{F}$, $\mathbf{a} = \mathbf{f}$, $\alpha = \phi$ and $\mathbf{B} = \mathbf{T}$, $\mathbf{b} = \mathbf{t}$ and $\beta = \tau(m_{m,\text{ref}})$,

where \mathbf{T} , \mathbf{t} and $\tau(m_{m,\text{ref}})$ are as in (9), $\mathbf{V}(\omega_k)$, $\mathbf{v}(\omega_k)$ and $\nu(\omega_k, \hat{u}_{\text{max}})$ as in (15) and \mathbf{F} , \mathbf{f} and ϕ as in (21). To obtain the optimal reference current vector as in (A3), the following necessary and sufficient conditions must be evaluated.

A.1.1. Necessary condition for a maximum. To find a maximum, the following *necessary* condition must be satisfied: The gradient⁵ of the Lagrangian must be equal to the zero vector, i.e.

$$\begin{aligned} \mathbf{g}_{\mathcal{L}}(\mathbf{i}_s^k, \lambda) &:= \left(\frac{d\mathcal{L}(\mathbf{i}_s^k, \lambda)}{d(\mathbf{i}_s^k, \lambda)} \right)^\top \\ &= \left(\left(\frac{d\mathcal{L}(\mathbf{i}_s^k, \lambda)}{d(\mathbf{i}_s^k, \lambda)} \right)^\top \right) \stackrel{!}{=} \mathbf{0}_3 \\ &\stackrel{(\text{A3})}{\Rightarrow} \left(\begin{array}{c} -2\mathbf{A}\mathbf{i}_s^k - 2\mathbf{a} + \lambda(2\mathbf{B}\mathbf{i}_s^k + 2\mathbf{b}) \\ (\mathbf{i}_s^k)^\top \mathbf{B} \mathbf{i}_s^k + 2\mathbf{b}^\top \mathbf{i}_s^k + \beta \end{array} \right) \stackrel{!}{=} \mathbf{0}_3. \end{aligned} \quad (\text{A5})$$

By defining

$$\begin{aligned} \mathbf{M}(\lambda) &:= \lambda \mathbf{B} - \mathbf{A} = \begin{bmatrix} \lambda b_{11} - a_{11} & \lambda b_{12} - a_{12} \\ \lambda b_{12} - a_{12} & \lambda b_{22} - a_{22} \end{bmatrix} \text{ and} \\ \mathbf{m}(\lambda) &:= \lambda \mathbf{b} - \mathbf{a} = \begin{pmatrix} \lambda b_1 - a_1 \\ \lambda b_2 - a_2 \end{pmatrix}, \end{aligned} \quad (\text{A6})$$

one may rewrite the first two rows in (A5) in the compact form

$$2[\lambda \mathbf{B} - \mathbf{A}] \mathbf{i}_s^k + (\lambda \mathbf{b} - \mathbf{a}) \stackrel{(\text{A6})}{=} 2\mathbf{M}(\lambda) \mathbf{i}_s^k + 2\mathbf{m}(\lambda) = \mathbf{0}_2 \quad (\text{A7})$$

and, solving for $\mathbf{i}_s^k = \mathbf{i}_s^{k,*}$, yields

$$\mathbf{i}_s^{k,*}(\lambda) = -[\lambda \mathbf{B} - \mathbf{A}]^{-1} (\lambda \mathbf{b} - \mathbf{a}) \stackrel{(\text{A6})}{=} -\mathbf{M}(\lambda)^{-1} \mathbf{m}(\lambda) \quad (\text{A8})$$

where

$$\begin{aligned} \mathbf{M}(\lambda)^{-1} &= [\lambda \mathbf{B} - \mathbf{A}]^{-1} \\ &= \frac{1}{\det \mathbf{M}(\lambda)} \begin{bmatrix} \lambda b_{22} - a_{22} & -\lambda b_{12} + a_{12} \\ -\lambda b_{12} + a_{12} & \lambda b_{11} - a_{11} \end{bmatrix} \\ &= ([\lambda \mathbf{B} - \mathbf{A}]^{-1})^\top = (\mathbf{M}(\lambda)^{-1})^\top \end{aligned}$$

and

$$\begin{aligned} \det \mathbf{M}(\lambda) &= (\lambda b_{11} - a_{11})(\lambda b_{22} - a_{22}) - (\lambda b_{12} - a_{12})^2 \\ &= (\det \mathbf{B}) \lambda^2 + (\det(\mathbf{B} - \mathbf{A}) - \det \mathbf{A} - \det \mathbf{B}) \lambda \\ &\quad + \det \mathbf{A}. \end{aligned}$$

Inserting $\mathbf{i}_s^k = \mathbf{i}_s^{k,*}(\lambda)$ as in (A8) into the constraint quadric $Q_B(\mathbf{i}_s^k)$ as in (A3) gives a *quartic polynomial* in λ as follows:

$$\left. \begin{aligned} &\mathbf{m}(\lambda)^\top \mathbf{M}(\lambda)^{-1} \mathbf{B} \mathbf{M}(\lambda)^{-1} \mathbf{m}(\lambda) \\ &- 2\mathbf{b}^\top \mathbf{M}(\lambda)^{-1} \mathbf{m}(\lambda) + \beta = 0 \\ &| \cdot \det(\mathbf{M}(\lambda))^2 \\ \implies &\chi_4(\lambda) := c_4 \lambda^4 + c_3 \lambda^3 \\ &\quad + c_2 \lambda^2 + c_1 \lambda + c_0 = 0 \end{aligned} \right\} \quad (\text{A9})$$

with *real coefficients*

$$\left. \begin{aligned} c_4 &:= -(b_{11} b_{22} - b_{12}^2) (b_{22} b_1^2 - 2b_1 b_2 b_{12} + b_{11} b_2^2 \\ &\quad + \beta b_{12}^2 - b_{11} b_{22} \beta) \\ c_3 &:= 2(a_{11} b_{22} - 2a_{12} b_{12} + a_{22} b_{11}) (b_{22} b_1^2 - 2b_1 b_2 b_{12} \\ &\quad + b_{11} b_2^2 + \beta b_{12}^2 - b_{11} b_{22} \beta) \\ c_2 &:= a_1^2 b_{11} b_{22}^2 - a_1^2 b_{12}^2 b_{22} - 2a_1 a_2 b_{11} b_{12} b_{22} + 2a_1 a_2 b_{12}^3 \\ &\quad - 2a_1 a_{11} b_1 b_{22}^2 + 2a_1 a_{11} b_2 b_{12} b_{22} + 4a_1 a_{12} b_1 b_{12} b_{22} \\ &\quad - 2a_1 a_{12} b_2 b_{11} b_{22} - 2a_1 a_{12} b_2 b_{12}^2 - 2a_1 a_{22} b_1 b_{12}^2 \\ &\quad + 2a_1 a_{22} b_2 b_{11} b_{12} + a_2^2 b_{11}^2 b_{22} - a_2^2 b_{11} b_{12}^2 \\ &\quad + 2a_2 a_{11} b_1 b_{12} b_{22} - 2a_2 a_{11} b_2 b_{12}^2 - 2a_2 a_{12} b_1 b_{11} b_{22} \\ &\quad - 2a_2 a_{12} b_1 b_{12}^2 + 4a_2 a_{12} b_2 b_{11} b_{12} + 2a_2 a_{22} b_1 b_{11} b_{12} \\ &\quad - 2a_2 a_{22} b_2 b_{11}^2 - a_{11}^2 b_2^2 b_{22} + \beta a_{11}^2 b_{22}^2 \\ &\quad + 2a_{11} a_{12} b_1 b_2 b_{22} + 2a_{11} a_{12} b_2^2 b_{12} - 4\beta a_{11} a_{12} b_{12} b_{22} \\ &\quad - 4a_{11} a_{22} b_1^2 b_{22} + 6a_{11} a_{22} b_1 b_2 b_{12} - 4a_{11} a_{22} b_2^2 b_{11} \\ &\quad + 4\beta a_{11} a_{22} b_{11} b_{22} - 2\beta a_{11} a_{22} b_{12}^2 + 3a_{12}^2 b_1^2 b_{22} \\ &\quad - 10a_{12}^2 b_1 b_2 b_{12} + 3a_{12}^2 b_2^2 b_{11} - 2\beta a_{12}^2 b_{11} b_{22} \\ &\quad + 6\beta a_{12}^2 b_{12}^2 + 2a_{12} a_{22} b_1^2 b_{12} + 2a_{12} a_{22} b_1 b_2 b_{11} \\ &\quad - 4\beta a_{12} a_{22} b_{11} b_{12} - a_{22}^2 b_1^2 b_{11} + \beta a_{22}^2 b_{11}^2 \\ c_1 &:= 2a_1^2 a_{22} b_{12}^2 - 2b_{11} b_{22} a_1^2 a_{22} - 4a_1 a_2 a_{12} b_{12}^2 \\ &\quad + 4b_{11} b_{22} a_1 a_2 a_{12} + 4b_{22} a_1 a_{11} a_{22} b_1 \\ &\quad - 4a_1 a_{11} a_{22} b_2 b_{12} - 4b_{22} a_1 a_{12}^2 b_1 \\ &\quad + 4a_1 a_{12}^2 b_2 b_{12} + 2a_2^2 a_{11} b_{12}^2 - 2b_{11} b_{22} a_2^2 a_{11} \\ &\quad - 4a_2 a_{11} a_{22} b_1 b_{12} + 4b_{11} a_2 a_{11} a_{22} b_2 \\ &\quad + 4a_2 a_{12}^2 b_1 b_{12} - 4b_{11} a_2 a_{12}^2 b_2 + 2a_{11}^2 a_{22} b_2^2 \\ &\quad - 2b_{22} \beta a_{11}^2 a_{22} - 2a_{11} a_{12}^2 b_2^2 + 2b_{22} \beta a_{11} a_{12}^2 \\ &\quad - 4a_{11} a_{12} a_{22} b_1 b_2 + 4\beta a_{11} a_{12} a_{22} b_{12} \\ &\quad + 2a_{11} a_{22}^2 b_1^2 - 2b_{11} \beta a_{11} a_{22}^2 \\ &\quad + 4a_{12}^3 b_1 b_2 - 4\beta a_{12}^3 b_{12} - 2a_{12}^2 a_{22} b_1^2 + 2b_{11} \beta a_{12}^2 a_{22} \\ c_0 &:= b_{22} a_1^2 a_{12}^2 - 2b_{12} a_1^2 a_{12} a_{22} + b_{11} a_1^2 a_{22}^2 \\ &\quad - 2b_{22} a_1 a_2 a_{11} a_{12} + 2b_{12} a_1 a_2 a_{11} a_{22} + 2b_{12} a_1 a_2 a_{12}^2 \\ &\quad - 2b_{11} a_1 a_2 a_{12} a_{22} + 2b_2 a_1 a_{11} a_{12} a_{22} - 2b_1 a_1 a_{11} a_{22}^2 \\ &\quad - 2b_2 a_1 a_{12}^3 + 2b_1 a_1 a_{12}^2 a_{22} + b_{22} a_2^2 a_{11}^2 \\ &\quad - 2b_{12} a_2^2 a_{11} a_{12} + b_{11} a_2^2 a_{12}^2 - 2b_2 a_2 a_{11}^2 a_{22} \\ &\quad + 2b_2 a_2 a_{11} a_{12}^2 + 2b_1 a_2 a_{11} a_{12} a_{22} - 2b_1 a_2 a_{12}^3 \\ &\quad + \beta a_{11}^2 a_{22}^2 - 2\beta a_{11} a_{12}^2 a_{22} + \beta a_{12}^4. \end{aligned} \right\} \quad (\text{A10})$$

A.1.2. Sufficient condition for a maximum. To obtain a *maximum* under an equality constraint, the Hessian of the Lagrangian $\mathcal{L}(\mathbf{i}_s^k, \lambda)$ must be *negative definite*, i.e.

$$\mathbf{H}_{\mathcal{L}}(\mathbf{i}_s^k, \lambda) := \frac{d}{d(\mathbf{i}_s^k, \lambda)} \left(\frac{d\mathcal{L}(\mathbf{i}_s^k, \lambda)}{d(\mathbf{i}_s^k, \lambda)} \right)^\top \stackrel{!}{<} 0. \quad (\text{A11})$$

The Hessian matrix is symmetric and given by

$$\begin{aligned} \mathbf{H}_{\mathcal{L}}(\mathbf{i}_s^k, \lambda) &:= \frac{d}{d(\mathbf{i}_s^k, \lambda)} \left(\frac{d\mathcal{L}(\mathbf{i}_s^k, \lambda)}{d(\mathbf{i}_s^k, \lambda)} \right)^\top \\ &= \begin{bmatrix} 2\mathbf{M}(\lambda) & 2\mathbf{B}\mathbf{i}_s^k + 2\mathbf{b} \\ (2\mathbf{B}\mathbf{i}_s^k + 2\mathbf{b})^\top & 0 \end{bmatrix} \\ &= \mathbf{H}_{\mathcal{L}}(\mathbf{i}_s^k, \lambda)^\top \in \mathbb{R}^{3 \times 3}. \end{aligned} \quad (\text{A12})$$

The Hessian $\mathbf{H}_{\mathcal{L}}(\mathbf{i}_s^k, \lambda)$ is negative definite if and only if all its leading principal minors⁶ have alternating

signs (see Bernstein, 2009, Proposition 8.2.8, in combination with Bernstein, 2009, Proposition 2.7.1⁷). More precisely, the first and third leading principle minor of (A12) must be *negative* whereas the second leading principle minor must be *positive*, i.e. $2m_{11}(\lambda^*) \stackrel{(A6)}{=} 2(a_{11} + \lambda^* b_{11}) < 0$ (the first leading principal minor), $\det(2\mathbf{M}(\lambda^*)) = 2^2 \det \mathbf{M}(\lambda^*) > 0$ (the second leading principal minor) and $\det(\mathbf{H}_{\mathcal{L}}(\mathbf{i}_s^k, \lambda^*)) < 0$ (the third leading principal minor). Hence, the optimal (real) Lagrangian multiplier $\lambda^* \in \mathbb{R}$ must satisfy

$$\left. \begin{array}{l} \text{(i) } \lambda^* < \frac{a_{11}}{b_{11}} \implies 2(\lambda^* b_{11} - a_{11}) < 0 \\ \text{(ii) } \lambda^* > \frac{(\det(\mathbf{B}-\mathbf{A}) - \det \mathbf{A} - \det \mathbf{B})}{-\text{sign}(\det \mathbf{B}) \det \mathbf{B}} \\ \quad \times \left(1 \pm \sqrt{1 - \frac{4 \det \mathbf{A} \det \mathbf{B}}{(\det(\mathbf{B}-\mathbf{A}) - \det \mathbf{A} - \det \mathbf{B})^2}} \right) \\ \implies \det \mathbf{M}(\lambda^*) > 0. \end{array} \right\} \quad (\text{A13})$$

Clearly, the conditions (i) and (ii) in (A13) must be satisfied simultaneously and, therefore, imply negative definiteness of $\mathbf{M}(\lambda^*) = \lambda^* \mathbf{B} - \mathbf{A}$. Moreover, by defining

$$\mathbf{C}(\mathbf{i}_s^k, \lambda^*) := \begin{bmatrix} \mathbf{I}_2, & \mathbf{M}(\lambda^*)^{-1}(\mathbf{B}\mathbf{i}_s^k + \mathbf{b}) \\ \mathbf{0}_2^\top, & 1 \end{bmatrix} \in \mathbb{R}^{3 \times 3}$$

with $\det \mathbf{C}(\mathbf{i}_s^k, \lambda^*) = \det \mathbf{C}(\mathbf{i}_s^k, \lambda^*)^\top = 1$ and, by invoking Bernstein (2009, Fact. 2.16.2), the Hessian matrix

$$\begin{aligned} \mathbf{H}_{\mathcal{L}}(\mathbf{i}_s^k, \lambda^*) \\ = 2\mathbf{C}(\mathbf{i}_s^k, \lambda^*)^\top \begin{bmatrix} \mathbf{M}(\lambda^*), & \mathbf{0}_2 \\ \mathbf{0}_2^\top, & -((\mathbf{i}_s^k)^\top \mathbf{B}^\top + \mathbf{b}^\top) \\ & \mathbf{M}(\lambda^*)^{-1}(\mathbf{B}\mathbf{i}_s^k + \mathbf{b}) \end{bmatrix} \mathbf{C}(\mathbf{i}_s^k, \lambda^*) \end{aligned} \quad (\text{A11})$$

can be written as the product of three matrices. Hence,

$$\begin{aligned} \det[\mathbf{H}_{\mathcal{L}}(\mathbf{i}_s^k, \lambda^*)] \\ = -2 \underbrace{((\mathbf{i}_s^k)^\top \mathbf{B}^\top + \mathbf{b}^\top) \mathbf{M}(\lambda^*)^{-1} (\mathbf{B}\mathbf{i}_s^k + \mathbf{b})}_{=: \gamma \in \mathbb{R}} \\ \cdot \det \mathbf{M}(\lambda^*), \end{aligned}$$

which, with $\det \mathbf{C}(\mathbf{i}_s^k, \lambda^*) = \det \mathbf{C}(\mathbf{i}_s^k, \lambda^*)^\top = 1$ and negative definiteness of $\mathbf{M}(\lambda^*) = [\mathbf{A} + \lambda^* \mathbf{B}] \stackrel{(A13)}{<} 0$, implies

that $\gamma = \|\mathbf{B}\mathbf{i}_s^k + \mathbf{b}\|_{\mathbf{M}(\lambda^*)}^2 < 0$ (a weighted norm with negative definite $\mathbf{M}(\lambda^*) < 0$) is negative for all *non-zero* vectors:

$$\begin{aligned} \mathbf{B}\mathbf{i}_s^{k,*}(\lambda^*) + \mathbf{b} &\stackrel{(A8)}{=} -\lambda^* \mathbf{B}[\mathbf{A} + \lambda^* \mathbf{B}]^{-1} \mathbf{b} + \mathbf{b} \\ &= -(-\mathbf{I}_2 + \lambda^* \mathbf{B}[\mathbf{A} + \lambda^* \mathbf{B}]^{-1}) \mathbf{b} \\ &= [\mathbf{A} + \lambda^* \mathbf{B}]^{-1} \mathbf{b} \\ &\stackrel{(A13)}{\neq} \mathbf{0}_2 \text{ for all } \lambda^* \text{ as in (A13),} \end{aligned}$$

where, in the second step, Corollary 2.8.10 from Bernstein (2009) was used. Concluding, for the optimal λ^* , the third leading principle minor is (always) negative, i.e. $\det[\mathbf{H}_{\mathcal{L}}(\mathbf{i}_s^k, \lambda^*)] < 0$. By checking definiteness of (A11) for $\lambda^* \in \{\lambda_1^*, \dots, \lambda_4^*\}$, where $\mathbf{M}(\lambda^*) > 0$, the analytical solution for the optimal reference current vector is finally given by

$$\begin{aligned} \mathbf{i}_{s,\text{ref}}^k &\stackrel{(A3)}{:=} \mathbf{i}_s^{k,*}(\lambda^*) \stackrel{(A8)}{=} -\mathbf{M}(\lambda^*)^{-1} \mathbf{m}(\lambda^*) \\ &= -[\lambda^* \mathbf{B} - \mathbf{A}]^{-1} (\lambda^* \mathbf{b} - \mathbf{a}). \end{aligned} \quad (\text{A14})$$

Remark A.1

(The case $\mathbf{m}(\lambda) = \mathbf{0}_2$ for all $\lambda \in \mathbb{C}$): Note that the optimal reference current vector (A14) only gives a non-trivial solution if $\mathbf{m}(\lambda) = \lambda \mathbf{b} - \mathbf{a} \neq 0$. This is not true for RSMs, where $\psi_{\text{pm}} = 0$ and, hence, $\mathbf{t} \stackrel{(9)}{=} \mathbf{0}_2$, $\mathbf{v}(\omega_k) \stackrel{(15)}{=} \mathbf{0}_2$ and $\mathbf{f} \stackrel{(21)}{=} \mathbf{0}_2$. To solve these optimisation problems, (A3) must be re-formulated by shifting/translating the quadrics $Q_A(\mathbf{i}_s^k)$ and $Q_B(\mathbf{i}_s^k)$ by some non-zero but constant $\mathbf{x}_s \in \mathbb{R}^2$. The shifted quadrics $Q_A(\mathbf{i}_s^k + \mathbf{x}_s)$ and $Q_B(\mathbf{i}_s^k + \mathbf{x}_s)$ are obtained by inserting $\mathbf{i}_s^k = \mathbf{i}_s^k + \mathbf{x}_s$ into (A3) (for more details, see Appendix A.4).

Remark A.2 (Normalisation): For a numerical implementation, a normalisation of (8) might be beneficial yielding a less ill-conditioned optimisation problem (the coefficients of the fourth-order polynomial (A9) heavily differ in magnitude). The normalised version of (8) is

$$\bar{\mathbf{u}}_s^k = \bar{R}_s \bar{\mathbf{i}}_s^k + \bar{\omega}_k \bar{\mathbf{J}} \bar{\mathbf{L}}_s^k \bar{\mathbf{i}}_s^k + \bar{\omega}_k \bar{\mathbf{J}} \bar{\boldsymbol{\psi}}_{\text{pm}}^k, \quad (\text{A15})$$

where the normalised (unitless) quantities and parameters are defined by $\bar{\mathbf{u}}_s^k := \frac{u_s^k}{\hat{u}_{\text{max}}}$, $\bar{R}_s := \frac{R_s}{\hat{u}_{\text{max}}/\hat{i}_{\text{max}}}$, $\bar{\mathbf{i}}_s^k := \frac{i_s^k}{\hat{i}_{\text{max}}}$, $\bar{\omega}_k := \frac{\omega_k}{\omega_{k,\text{nom}}}$, $\bar{\mathbf{L}}_s^k := \frac{\omega_{k,\text{nom}}}{\hat{u}_{\text{max}}/\hat{i}_{\text{max}}} \mathbf{L}_s^k$ and $\bar{\boldsymbol{\psi}}_{\text{pm}}^k := \frac{\omega_{k,\text{nom}}}{\hat{u}_{\text{max}}} \boldsymbol{\psi}_{\text{pm}}^k$. The normalised (unitless) machine torque and its reference are as follows:

$$\begin{aligned} \bar{m}_m &:= \frac{\omega_{k,\text{nom}}}{\hat{u}_{\text{max}} \hat{i}_{\text{max}}} m_m \quad \text{and} \\ \bar{m}_{m,\text{ref}} &:= \frac{\omega_{k,\text{nom}}}{\hat{u}_{\text{max}} \hat{i}_{\text{max}}} m_{m,\text{ref}}. \end{aligned}$$

A.1.3. Analytical computation of the roots of a quartic polynomial. The discriminant of the quartic polynomial $\chi_4(\lambda)$ as in (A9) can be computed as follows:

$$\begin{aligned} \Delta := & 256c_4^3c_0^3 - 192c_4^2c_3c_1c_0^2 - 128c_4^2c_2^2c_0^2 + 144c_4^2c_2c_1^2c_0 \\ & - 27c_4^2c_1^4 + 144c_4c_3^2c_2c_0^2 - 6c_4c_3^2c_1^2c_0 - 80c_4c_3c_2^2c_1c_0 \\ & + 18c_4c_3c_2c_1^3 + 16c_4c_2^4c_0 - 4c_4c_2^3c_1^2 - 27c_3^4c_0^2 \\ & + 18c_3^3c_2c_1c_0 - 4c_3^3c_1^3 - 4c_3^2c_2^3c_0 + c_3^2c_2^2c_1^2. \end{aligned} \quad (\text{A16})$$

For $\Delta < 0$, the quartic polynomial (A9) has two real and two complex roots (all distinct); for $\Delta > 0$, (A9) has four real or four complex roots (all distinct) and, for $\Delta = 0$, (A9) has at least two equal roots (for more details, see Rees, 1922). Euler's solution will be presented (for details, see Nickalls, 2009) which is based on the *depressed* (and monic) quartic polynomial given by

$$\chi_{4,\text{dep}}(y) := y^4 + py^2 + qy + r = 0 \quad (\text{A17})$$

with real coefficients

$$\begin{aligned} p &:= \frac{1}{c_4} \left(c_2 c_4 - \frac{3c_3^2}{8} \right), \\ q &:= \frac{1}{c_4^3} \left(\frac{c_3^3}{8} - \frac{c_2 c_3 c_4}{2} + c_1 c_4^2 \right) \& \\ r &:= \frac{1}{c_4^4} \left(-\frac{3c_3^4}{256} + c_4^3 c_0 - \frac{c_4^2 c_3 c_2}{4} + \frac{c_4 c_3^2 c_2}{16} \right). \end{aligned} \quad (\text{A18})$$

The depressed quartic polynomial (A17) is obtained by inserting $\lambda := y - \frac{c_3}{4c_4}$ into (A9). To compute the roots of the depressed quartic, one needs to find the three roots z_1^* , z_2^* and z_3^* of Euler's resolvent cubic polynomial given by

$$\chi_{3,\text{res}}(z) := z^3 + 2pz^2 + (p^2 - 4r)z - q^2 = 0, \quad (\text{A19})$$

where p , q and r are as in (A18). In Appendix A.1.4, the analytical solution to compute the three roots z_1^* , z_2^* and z_3^* of the resolvent cubic (A19) is presented. Finally, for known resolvent roots z_1^* , z_2^* and z_3^* , the four roots λ_1^* , λ_2^* , λ_3^* and λ_4^* of the quartic polynomial (A9) are given by

$$\left. \begin{aligned} \lambda_1^* &= \frac{(-1)^l}{2} \left(\sqrt{z_1^*} + \sqrt{z_2^*} + \sqrt{z_3^*} \right) - \frac{c_3}{4c_4}, \\ \lambda_2^* &= \frac{(-1)^l}{2} \left(\sqrt{z_1^*} - \sqrt{z_2^*} - \sqrt{z_3^*} \right) - \frac{c_3}{4c_4}, \\ \lambda_3^* &= \frac{(-1)^l}{2} \left(-\sqrt{z_1^*} + \sqrt{z_2^*} - \sqrt{z_3^*} \right) - \frac{c_3}{4c_4}, \\ \lambda_4^* &= \frac{(-1)^l}{2} \left(-\sqrt{z_1^*} - \sqrt{z_2^*} + \sqrt{z_3^*} \right) - \frac{c_3}{4c_4}, \end{aligned} \right\} \text{and} \quad (\text{A20})$$

where $l \in \{0, 1\}$ must be chosen such that (Nickalls, 2009)

$$(-1)^l (\lambda_1^* \lambda_2^* \lambda_3^* + \lambda_1^* \lambda_2^* \lambda_4^* + \lambda_1^* \lambda_3^* \lambda_4^* + \lambda_2^* \lambda_3^* \lambda_4^*) = -q.$$

A.1.4. Analytical computation of the roots of a cubic polynomial. Consider the monic cubic polynomial with real coefficients given by

$$\begin{aligned} \chi_3(z) := & z^3 + d_2z^2 + d_1z + d_0 = 0 \quad \text{where} \\ & d_2, \dots, d_0 \in \mathbb{R}. \end{aligned} \quad (\text{A21})$$

Its roots z_1^* , z_2^* and z_3^* can be computed analytically as described in the following paragraph (Abramowitz, Stegun, & Miller, 1964, p. 17). Note that the cubic polynomial $\chi_3(z)$ has (a) one real and a pair of complex conjugate roots if $\tilde{q}^3 + \tilde{r}^2 > 0$, (b) only real roots but at least two are equal if $\tilde{q}^3 + \tilde{r}^2 = 0$, and (c) only real roots but all are distinct if $\tilde{q}^3 + \tilde{r}^2 < 0$. For the following, define

$$\tilde{q} := \frac{d_1}{3} - \frac{d_2^2}{9} \quad \text{and} \quad \tilde{r} := \frac{d_1d_2 - 3d_0}{6} - \frac{d_2^3}{27}.$$

Then, for

$$\begin{aligned} s_1 &:= \sqrt{3\tilde{r}} + \sqrt{\tilde{q}^3 + \tilde{r}^2} \quad \text{and} \\ s_2 &:= \sqrt{3\tilde{r}} - \sqrt{\tilde{q}^3 + \tilde{r}^2}, \end{aligned}$$

the three roots of the cubic polynomial (A21) are given by

$$\begin{aligned} z_1^* &= (s_1 + s_2) - \frac{d_2}{3} \quad \text{and} \\ z_{2,3}^* &= -\frac{1}{2}(s_1 + s_2) - \frac{d_2}{3} \pm j \frac{\sqrt{3}}{2}(s_1 - s_2). \end{aligned} \quad (\text{A22})$$

Appendix 2. Computation of the quadrics (implicit expressions) for MTPC, MTPV and MTPF

To derive the implicit forms for the MTPC, MTPV and MTPF hyperbolas presented in Section 3.2, the first two rows of the gradient (A5) must be set to zero, i.e.

$$\begin{aligned} -\mathbf{A}_s^k - \mathbf{a} + \lambda(\mathbf{B}_s^k + \mathbf{b}) &= \mathbf{0}_2 \\ \implies \lambda \begin{pmatrix} (b_{11}, b_{12})_s^k + b_1 \\ (b_{12}, b_{22})_s^k + b_2 \end{pmatrix} &= \begin{pmatrix} (a_{11}, a_{12})_s^k + a_1 \\ (a_{12}, a_{22})_s^k + a_2 \end{pmatrix}. \end{aligned} \quad (\text{A23})$$

Rewriting this equation componentwise, one may solve for and eliminate the Lagrangian multiplier λ as follows:

$$\begin{aligned}\lambda &= \frac{(a_{11}, a_{12})\mathbf{i}_s^k + a_1}{(b_{11}, b_{12})\mathbf{i}_s^k + b_1} = \frac{(a_{12}, a_{22})\mathbf{i}_s^k + a_2}{(b_{12}, b_{22})\mathbf{i}_s^k + b_2} \\ \implies &((a_{11}, a_{12})\mathbf{i}_s^k + a_1)((b_{12}, b_{22})\mathbf{i}_s^k + b_2) \\ &- ((a_{12}, a_{22})\mathbf{i}_s^k + a_2)((b_{11}, b_{12})\mathbf{i}_s^k + b_1) = 0.\end{aligned}\quad (\text{A24})$$

Re-arranging leads to the following quadric:

$$(\mathbf{i}_s^k)^\top \mathbf{M}_X \mathbf{i}_s^k + 2\mathbf{m}_X^\top \mathbf{i}_s^k + \mu_X$$

where the respective matrix, vector and scalar are as follows:

$$\left. \begin{aligned}\mathbf{M}_X &= \mathbf{M}_X^\top \\ &\stackrel{(\text{A2})}{=} \begin{bmatrix} a_{11}b_{12} - a_{12}b_{11} & \frac{1}{2}(a_{11}b_{22} - a_{22}b_{11}) \\ \frac{1}{2}(a_{11}b_{22} - a_{22}b_{11}) & a_{12}b_{22} - a_{22}b_{12} \end{bmatrix}, \\ \mathbf{m}_X &= \frac{1}{2} \begin{pmatrix} a_{11}b_2 + a_1b_{12} - a_{12}b_1 - a_2b_{11} \\ a_{12}b_2 + a_1b_{22} - a_{22}b_1 - a_2b_{12} \end{pmatrix} \\ \mu_X &= a_1b_2 - a_2b_1.\end{aligned}\right\} \text{ and } \quad (\text{A25})$$

The corresponding matrix \mathbf{M}_X , vector \mathbf{m}_X and scalar μ_X in (A23) with $X \in \{C, V, F\}$ are obtained for

- the MTPC hyperbola (23) (i.e. $X = C$) by setting $\mathbf{A} = \mathbf{I}_2$, $\mathbf{a} = (0, 0)^\top$, $\mathbf{B} = \mathbf{T}$ and $\mathbf{b} = \mathbf{t}$;
- the MTPV hyperbola (29) (i.e. $X = V$) by setting $\mathbf{A} = \mathbf{V}(\omega_k)$, $\mathbf{a} = \mathbf{v}(\omega_k)$, $\mathbf{B} = \mathbf{T}$ and $\mathbf{b} = \mathbf{t}$; and
- the MTPF hyperbola (33) (i.e. $X = F$) by setting $\mathbf{A} = \mathbf{F}$, $\mathbf{a} = \mathbf{f}$, $\mathbf{B} = \mathbf{T}$ and $\mathbf{b} = \mathbf{t}$,

with \mathbf{T} and \mathbf{t} as in (9), $\mathbf{V}(\omega_k)$ and $\mathbf{v}(\omega_k)$ as in (15) and \mathbf{f} as in (21), respectively.

Appendix 3. Explicit expressions for current circle, voltage ellipse, and torque, MTPC, MTPV and MTPF hyperbolas

Consider an arbitrary quadric $Q_A(\mathbf{i}_s^k)$ as in (A1), where \mathbf{A} , \mathbf{a} (and their respective entries a_{ij} and a_i) and α are as in (A2). An explicit expression for $Q_A(\mathbf{i}_s^k)$ can be obtained by solving $Q_A(\mathbf{i}_s^k)$ as in (A1) for the quadrature current i_s^q . To derive an explicit expression, different cases must be taken into account (like signs or whether certain parameters are zero or not) which makes the use of explicit expressions tedious. Assuming the explicit expression

of the quadric $Q_A(\mathbf{i}_s^k)$ as in (A1) exists, it is given by

$$\mathbb{A}(i_s^d) = -\frac{a_{12}i_s^d + a_2}{a_{22}} \pm \frac{\sqrt{(a_{12}i_s^d + a_2)^2 - a_{22}(a_{11}(i_s^d)^2 + 2a_1i_s^d + \alpha)}}{a_{22}}. \quad (\text{A26})$$

Clearly, to have a meaningful expression, the following must hold: $a_{22} \neq 0$ and $(a_{12}i_s^d + a_2)^2 - a_{22}(a_{11}(i_s^d)^2 + 2a_1i_s^d + \alpha) \geq 0$ for all $i_s^d \in \mathbb{R}$ (which might not hold in general; leading to different cases where (A26) will hold). To compute the explicit expressions for torque, current circle, voltage ellipse, MTPC, MTPV or MTPF hyperbola, the corresponding matrix \mathbf{A} , vector \mathbf{a} and scalar α must be chosen accordingly (e.g. for the voltage ellipse (17), choose $\mathbf{A} = \mathbf{V}(\omega_k)$, $\mathbf{a} = \mathbf{v}(\omega_k)$ and $\alpha = v(\omega_k, \hat{u}_{\max})$ with $\mathbf{V}(\omega_k)$, $\mathbf{v}(\omega_k)$ and $v(\omega_k, \hat{u}_{\max})$ as in (15)).

Appendix 4. Computation of the intersection points of two arbitrary quadrics

To find the intersection point(s) \mathbf{x}^* of two arbitrary quadrics $Q_A(\mathbf{x})$ and $Q_B(\mathbf{x})$ as in (A1), there are several possible algorithms. In this paper, an algorithm is presented which leads to a problem of 'finding the roots of a fourth-order polynomial' again, and hence can be solved analytically (see Section A.1.3). For the following, introduce

$$\begin{aligned}\mathbf{D} &:= \begin{bmatrix} d_{11} & d_{12} \\ d_{12} & d_{22} \end{bmatrix} \in \mathbb{R}^{2 \times 2}, \quad \mathbf{d} := \begin{pmatrix} d_1 \\ d_2 \end{pmatrix} \in \mathbb{R}^2, \quad \mathbf{x}_s \in \mathbb{R}^2, \\ \mathbf{M} &:= \begin{bmatrix} m_{11} & m_{12} \\ m_{12} & m_{22} \end{bmatrix} \in \mathbb{R}^{2 \times 2}, \quad \mathbf{m} := \begin{pmatrix} m_1 \\ m_2 \end{pmatrix} \in \mathbb{R}^2, \quad \text{and } \mu \in \mathbb{R}\end{aligned}$$

and the quadric

$$Q_M(\mathbf{x}) := \mathbf{x}^\top \mathbf{M} \mathbf{x} + 2\mathbf{m}^\top \mathbf{x} + \mu. \quad (\text{A27})$$

To compute the analytical solutions of the intersection points of the quadrics $Q_A(\mathbf{x})$ and $Q_B(\mathbf{x})$, three different cases must be considered:

- If $\alpha \neq 0$ and $\beta \neq 0$ in (A1), then define the difference quadric of the scaled quadrics as follows:

$$\begin{aligned}Q_D(\mathbf{x}) &:= \frac{Q_A(\mathbf{x})}{\alpha} - \frac{Q_B(\mathbf{x})}{\beta} = \mathbf{x}^\top \mathbf{D} \mathbf{x} + 2\mathbf{d}^\top \mathbf{x} \\ &= \mathbf{x}^\top \left(\frac{\mathbf{A}}{\alpha} - \frac{\mathbf{B}}{\beta} \right) \mathbf{x} + 2 \left(\frac{\mathbf{a}}{\alpha} - \frac{\mathbf{b}}{\beta} \right)^\top \mathbf{x} = 0,\end{aligned}\quad (\text{A28})$$

where $\mathbf{D} := \left(\frac{\mathbf{A}}{\alpha} - \frac{\mathbf{B}}{\beta} \right)$ and $\mathbf{d} := \left(\frac{\mathbf{a}}{\alpha} - \frac{\mathbf{b}}{\beta} \right)$ and set $\mathbf{M} := \mathbf{A}$, $\mathbf{m} := \mathbf{a}$ and $\mu := \alpha$ (or $\mathbf{M} := \mathbf{B}$, $\mathbf{m} := \mathbf{b}$

and $\mu := \beta$ in (A27)). Both are possible and do not alter the result.

- (ii) If $\alpha = 0$ and $\beta \neq 0$ in (A1), then set $D := A, d := a$ in (A28), and $M := B, m := b$ and $\mu := \beta$ in (A27); or
if $\alpha \neq 0$ and $\beta = 0$ in (A1), then set $D := B, d := b$ in (A28), and $M := A, m := a$ and $\mu := \alpha$ in (A27).
- (iii) If $\alpha = 0$ and $\beta = 0$ in (A1), the quadrics $Q_A(x)$ and $Q_B(x)$ must be shifted (translated) by $x_s \in \mathbb{R}^2 \setminus \{0_2\}$ by inserting $x := y + x_s$ into (A1), i.e.

$$\begin{aligned}
 Q_A(y + x_s) &:= y^\top A y + 2 \underbrace{(x_s^\top A + a^\top)}_{=: a_s^\top} y \\
 &\quad + \underbrace{x_s^\top A x_s + 2 a^\top x_s}_{\alpha_s} \text{ and} \\
 Q_B(y + x_s) &:= y^\top B y + 2 \underbrace{(x_s^\top B + b^\top)}_{=: b_s^\top} y \\
 &\quad + \underbrace{x_s^\top B x_s + 2 b^\top x_s}_{\beta_s},
 \end{aligned}$$

such that the shifted scalars α_s and β_s are non-zero, i.e. $\alpha_s \neq 0$ and $\beta_s \neq 0$. Then, case (i) holds true again (but now in y) and one sets $D := (\frac{A}{\alpha_s} - \frac{B}{\beta_s})$, $d := (\frac{a_s}{\alpha_s} - \frac{b_s}{\beta_s})$ in (A28), and $M := A, m := a_s$ and $\mu := \alpha_s$ (or $M := B, m := b_s$ and $\mu := \beta_s$) in (A27). Finally, to obtain the intersections points x^* , the solution y^* must be translated again, i.e. $x^* = y^* + x_s$.

Note that, for all three cases (i), (ii) and (iii),⁸ $D = D^\top$ and one may rewrite (A28) as follows:

$$Q_D(x) = x^\top D x + 2 d^\top x = x^\top \underbrace{(D x + 2 d)}_{\stackrel{\perp}{=} \gamma J x} = 0. \quad (A29)$$

Since the vectors Jx (or $J^\top x$) and x are perpendicular to each other, the following holds $\gamma(Jx)^\top x = \gamma x^\top J^\top x = 0 = \gamma x^\top Jx$ for all $\gamma \in \mathbb{R} \setminus \{0\}$, and so (A29) is clearly satisfied for $Dx + 2d \stackrel{\perp}{=} \gamma Jx$ (the factor γ is necessary to

allow for scaled versions of the vector Jx ; such that different lengths are admissible). Hence, one obtains

$$\begin{aligned}
 [D - \gamma J]x + 2d = 0_2 &\implies x(\gamma) = -2[D - \gamma J]^{-1}d \\
 \text{where } [D - \gamma J]^{-1} &= \frac{1}{\gamma^2 + d_{11}d_{22} - d_{12}^2} \begin{bmatrix} d_{22} & -d_{12} - \gamma \\ \gamma - d_{12} & d_{11} \end{bmatrix}.
 \end{aligned}$$

Inserting $x(\gamma)$ as above into the quadric $Q_M(x)$ as in (A27) gives a fourth-order polynomial in γ , i.e.

$$\begin{aligned}
 4d^\top [D - \gamma J]^{-\top} M [D - \gamma J]^{-1} d - 4m^\top [D - \gamma J]^{-1} d \\
 + \mu = 0 \quad | \cdot (\det [D - \gamma J])^2 \\
 \implies \chi_4(\gamma) := \xi_4 \gamma^4 + \xi_3 \gamma^3 + \xi_2 \gamma^2 + \xi_1 \gamma + \xi_0 = 0
 \end{aligned} \quad (A30)$$

with coefficients

$$\left. \begin{aligned}
 \xi_4 &:= \mu \\
 \xi_3 &:= 4(m_1 d_2 - m_2 d_1) \\
 \xi_2 &:= 4 m_{22} d_1^2 d_2^2 - 8 m_{12} d_1 d_2 d_{12} + 4 m_2 d_1 d_{12} \\
 &\quad - 4 m_1 d_{22} d_1 + 4 m_{11} d_2^2 + 4 m_1 d_2 d_{12} \\
 &\quad - 4 m_2 d_{11} d_2 - 2 \mu d_{12}^2 + 2 \mu d_{11} d_{22} \\
 \xi_1 &:= 4 m_2 d_1 d_{12}^2 - 4 m_1 d_2 d_{12}^2 + 8 m_{11} d_2^2 d_{12} \\
 &\quad - 8 m_{12} d_2^2 d_{11} + 8 m_{12} d_1^2 d_{22} - 8 m_{22} d_1^2 d_{12} \\
 &\quad + 4 m_1 d_2 d_{11} d_{22} - 4 m_2 d_1 d_{11} d_{22} \\
 &\quad - 8 m_{11} d_1 d_2 d_{22} + 8 m_{22} d_1 d_2 d_{11} \\
 \xi_0 &:= 4 m_{22} d_1^2 d_{12}^2 - 8 m_{12} d_1^2 d_{12} d_{22} + 4 m_{11} d_1^2 d_{22}^2 \\
 &\quad - 8 m_{22} d_1 d_2 d_{11} d_{12} + 8 m_{12} d_1 d_2 d_{11} d_{22} \\
 &\quad + 8 m_{12} d_1 d_2 d_{12}^2 - 8 m_{11} d_1 d_2 d_{12} d_{22} \\
 &\quad + 4 m_2 d_1 d_{11} d_{12} d_{22} - 4 m_1 d_1 d_{11} d_{22}^2 \\
 &\quad - 4 m_2 d_1 d_{12}^3 + 4 m_1 d_1 d_{12}^2 d_{22} + 4 m_{22} d_2^2 d_{11}^2 \\
 &\quad - 8 m_{12} d_2^2 d_{11} d_{12} + 4 m_{11} d_2^2 d_{12}^2 \\
 &\quad - 4 m_2 d_2 d_{11}^2 d_{22} + 4 m_2 d_2 d_{11} d_{12}^2 \\
 &\quad + 4 m_1 d_2 d_{11} d_{12} d_{22} - 4 m_1 d_2 d_{12}^3 \\
 &\quad + \mu d_{11}^2 d_{22}^2 - 2 \mu d_{11} d_{12}^2 d_{22} + \mu d_{12}^4.
 \end{aligned} \right\} \quad (A31)$$

The real root γ^* of the four roots $\gamma_1^*, \gamma_2^*, \gamma_3^*, \gamma_4^*$ of the fourth-order polynomial $\chi_4(\gamma)$ as in (A30) gives the desired intersection point in the quadrant of interest, i.e.

$$\left. \begin{aligned}
 \text{for cases (i) and (ii): } x^*(\gamma^*) &= -2[D - \gamma^* J]^{-1}d, \text{ and } \\
 \text{for case (iii): } x^*(\gamma^*) &= -2[D - \gamma^* J]^{-1}d + x_s.
 \end{aligned} \right\} \quad (A32)$$

Note that there exist one, two, three or four real roots $\gamma_1^*, \gamma_2^*, \gamma_3^*, \gamma_4^*$ if the quadrics $Q_A(x)$ and $Q_B(x)$ do intersect; if the quadrics do not intersect, there is no real root.